Escuela Politécnica Nacional

FACULTAD DE INGENIERÍA MECANICA

DISEÑO DE ALABES DIRECTORES DE TURBINAS TIPO FRANCIS PARA MINIMIZAR LA EROSIÓN PRODUCIDA POR EL IMPACTO DEL FLUJO BIFÁSICO LÍQUIDO-SÓLIDO

QUISHPE CHOLANGO LUIS MIGUEL
luis.quishpe@epn.edu.ec

DIRECTOR
Ing. CANDO NARVAEZ EDGAR HERNAN, Ph.D.
edgar.cando@epn.edu.ec

CO-DIRECTOR
Ing. VALENCIA TORRES ESTEBAN ALEJANDRO, Ph.D.
esteban.valencia@epn.edu.ec

PROYECTO PREVIO A LA OBTENCIÓN DEL TÍTULO DE INGENIERO MECÁNICO

Quito, Septiembre, 2021

CERTIFICACIÓN

Certifico que el presente trabajo fue desarrollado por **LUIS MIGUEL QUISHPE CHOLANGO**, bajo mi supervision.

Ing. Cando Narvaez Edgar Hernan, Ph.D.
DIRECTOR DE PROYECTO

Ing. Valencia Torres Esteban Alejandro, Ph.D.
CODIRECTOR DE PROYECTO

DECLARACIÓN

Yo, **LUIS MIGUEL QUISHPE CHOLANGO**, declaro bajo juramento que el trabajo aquí descrito es de mi autoría; que no ha sido previamente presentado para ningún grado o calificación profesional; y, que he consultado las referencias bibliográficas que se incluyen en este documento.

A través de la presente declaración cedo mis derechos de propiedad intelectual correspondiente a este trabajo, a la Escuela Politécnica Nacional, según lo establecido por la Ley de Propiedad Intelectual, por su Reglamento y por la normativa institucional vigente.

Luis Miguel Quishpe Cholango

DEDICATORIA

A mi madre:
Que siempre me dio la libertad de poder elegir y hasta ahora lo hace. Esa libertad que siempre me ha llevado ha hacer todo lo que quiero.
A mi hermana Silvana Quishpe que siempre me llevo de la mano en todo lo que quise involucrarme.

AGRADECIMIENTO

A la Escuela Politécnica Nacional, por haberme formado y despertado mi interes por la Ingeniería Mecánica

A mi director, Edgar Cando, el cual es un excelente profesor un elemento de la sociedad invaluable.

A el proyecto PIS 19-06 por haberme dado todas las facilidades del caso para realizar el presente trabajo.

A mis amigos del día a día. Por su lealtad y respaldo.

CONTENTS

LIST OF FIGURES

LIST OF TABLES

ABSTRACT

Francis turbines are part of the main hydropower plants in Ecuador. Currently, more than half of the electrical energy comes from hydraulic sources in the country. The present work focuses on the design of guide vanes of Francis turbines to minimize erosion. A parametric modeling is performed with the data obtained from CELEC E.P. San Francisco hydroelectric plant, which is the case study. In addition, different profiles of NACA are analyzed. The drag they generate and the possible erosion of the runner blades are verified by dimensionless numbers. The NACA profile that minimizes erosion is selected, the 3D model of the turbine is obtained using computational tools. Through a numerical analysis with the use of commercial CFD codes, erosion caused by sediments in the guide vanes and runner blades is verified. The results show that the asymmetric profiles reduce the erosion in the guide vanes and runner blades.

RESUMEN

Las turbinas Francis forman parte de las principales centrales hidroeléctricas del Ecuador. Actualmente, más de la mitad de la energía eléctrica proviene de fuentes hidráulicas en el país. El presente trabajo se centra en el diseño de álabes directores de las turbinas Francis para minimizar la erosión. Se realiza un modelado paramétrico con los datos obtenidos de CELEC E.P. Central hidroeléctrica San Francisco que es el caso de estudio. Además, se analizan diferentes perfiles de NACA. El arrastre que generan y la posible erosión del corredor se verifican mediante números adimensionales. Se selecciona el perfil NACA que minimiza la erosión, el modelo 3D de la turbina se obtiene mediante herramientas computacionales. Mediante un análisis numérico con el uso de códigos CFD comerciales, se verifica la erosión provocada por sedimentos en las alabes directores y alabes del rodete. Los resultados muestran que los perfiles asimétricos reducen la erosión en los alabes directores y alabes del rodete.

INTRODUCTION

DISEÑO DE ALABES DIRECTORES DE TURBINAS TIPO FRANCIS PARA MINIMIZAR LA EROSIÓN PRODUCIDA POR EL IMPACTO DEL FLUJO BIFÁSICO LÍQUIDO-SÓLIDO

The erosion is produced by the impact of the liquid-solid two-phase flow on the elements of hydraulic machinery. Occurs due to the presence of sediments (high and low hardness particulate matter) present in the main rivers where hydroelectric plants are located along the Andes Mountains from Colombia to Chile [44]. Solid urban waste, volcanic particles and suspended sediments which are dragged by the river [45], cause accelerated wear on the guide vanes, due to the impact of the solid particles in suspension. There are several alternatives to reduce wear, most of which imply extremely high costs and these procedures are not very effective [46]. Efforts have been made to predict erosion areas in Francis turbines, which are ideal for the geography of Ecuador [6]. Understanding the phenomenon has been one of the greatest challenges for researchers worldwide. However, little has been done in Ecuador for the existing infrastructure. It is extremely important to promote improvements in machinery designs since energy consumption grows year after year in proportion to population growth.

Yánez (2017), when making parametric designs of the runner blade taking into account the reduction of erosion obtains satisfactory results showing that erosion affects each place where the working fluid comes into contact with the different elements [47]. Bone (2017) evaluating multi-objective optimization methodologies by genetic algorithms in the design of the runner blades chooses the design of it that reduces the tendency to erode. His results were verified using CFX [16]. Despite the efforts made, there are great obstacles since the phenomenon is not fully understood in the guide vanes. A parametric design of the guide vane is proposed. A structured mesh is made. Using commercial software to predict the erosion points through numerical simulation. Evaluation of the design verifying the reduction of the wear process due to erosion. The results obtained will allow decision-making regarding the operation of the turbomachine and other activities related to the operation of a hydroelectric plant.

In Ecuador, since 2007, a plan to guarantee the supply of electricity began. The use of sustainable sources over the years has been part of the generation system. In the vast

Figure 1: San Francisco Hydropower plant (Source:[43])

majority of hydroelectric power plants the use of Francis turbines has predominated. The Mazar, Agoyan, San Francisco, Sopladora and Marcel Laniado plants contribute to the Sistema Nacional Interconectado with an effective power of 60.75% in proportion to the total effective power nationwide. The country has a nominal power of 5066.40 MW and an effective power of 5036.43 MW, representing 96.2% in its effective power of all renewable energy in the country.

Hydroelectric plants are installed Ecuador´s three regions: coast (2 provinces), sierra (9 provinces) and Amazon (4 provinces) some are located in a mountainous region along the sierra and Amazon region. The hydroelectric power plants: Coca Codo Sinclair, Pucará, Agoyán, San Francisco, Mazar, Sopladora, Paute, Minas de San Francisco and Delsitanisagua [3], the plants are located in places where the working fluid comes from the Andes region loaded with particulate matter produced by volcanic eruptions, geological faults and even domestic plastic waste which erodes the components of hydraulic machinery and shorten their lifetime. High replacement and maintenance costs are another consequence of this phenomenon.[45]. Getting Francis turbine designs in line with reality while keeping costs low is an inherent need that must be addressed. Computational tools allow the study of models under different conditions, keeping costs low and providing promising results, establishing a clearer path for the development of future studies with substantial improvements over time.

OBJECTIVES

General objective

Design Francis-turbine-type guide vanes to minimize the erosion produced by the impact of the liquid-solid two-phase flow.

Specific Objectives

- Carry out a survey of the state of the art regarding the design of the guide vanes and studies to minimize erosion due to the impact of the liquid-solid two-phase flow in Francis turbines;

- Determine the parameters that influence the operation of the guide vanes and the erosion produced by the impact of the liquid-solid two-phase flow in Francis-type turbines;

- Establish a parametric and high-fidelity design methodology for guide vanes using computational fluid mechanics based on the functional requirements of the turbine and erosion produced by the impact of the liquid-solid two-phase flow;

- Validate the design methodology by comparing the data obtained with experimental results from previous studies;

- Define the optimal settings to reduce erosion processes at the best efficiency point.

SCOPE

In the present work the design of the the guide vanes of a Francis turbines is carried out. A review of the state of the art regarding the topic is performed. Parametric modeling is performed to obtain the main parameters of the Francis turbine of the case study. When selecting the profile of the guide vanes, a methodology with a two-dimensional approach is used. Different NACA profiles are analyzed using dimensionless numbers. Drag and erosion are part of the initial analysis. Once the profile is selected, the construction of the 3D computational model of the Francis turbine is carried out. Through numerical analysis with the use of computational tools erosion is verified in guide vanes and runner blades.

Chapter 1

THEORETICAL FRAMEWORK

1.1 Hydroelectric generation in Ecuador

Ecuador has a considerable amount of water resources. These resources are mostly in the Andes mountain range, the rest in the coastal and Amazon region. The country has 29 water systems made up of 79 basins. It has been estimated that there is a water potential of 22,500 [MW] and only 8% has been used.

Until 2017, the generation capacity was recorded at 7,434.81 [MW] of effective power. Of this amount, 4676.05 [MW] correspond to renewable energies. The energy from hydroelectric power plants corresponds to 4,486.41 [MW] [3].

In other words, renewable energies have a participation of 60.75% of the total national nominal power. In figure 1.1, it can be seen that hydroelectric power is the predominant source of electrical energy.

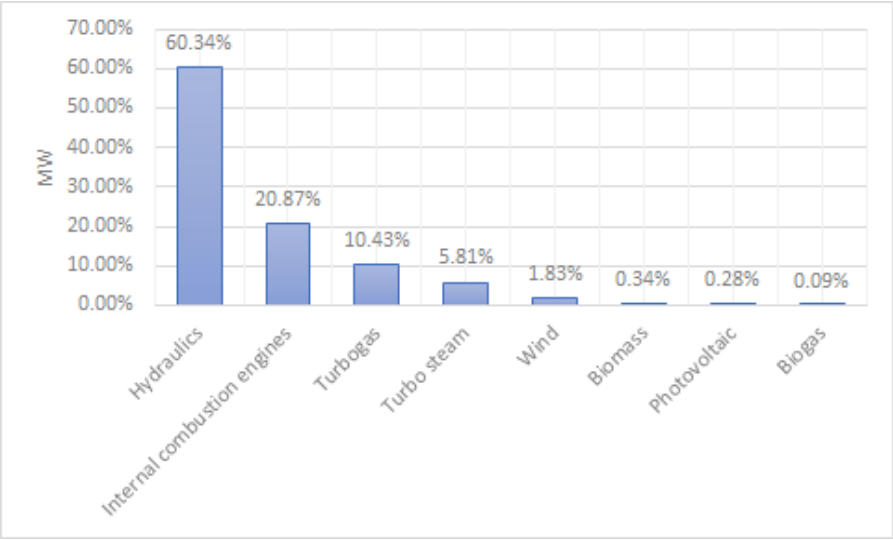

Figure 1.1: Gross energy production (Source:[2])

When analyzing the scenario by province, the largest participation is from the provinces of Azuay, Napo and Tungurahua. These three provinces account for 58.26% of the total energy production.Table 1.1 shows the gross energy production by province.

Table 1.1: Energy production by province (Source:[2])

Energy production by province			
Province	Production [MWh]	Province	Production [MWh]
Azuay	7.757.695,64	Cañar	317.072,46
Napo	6.139.496,63	Los Ríos	246.819,96
Tungurahua	2.605.223,44	Pastaza	227.302,15
Guayas	2.421.468,75	Santa Elena	218.778,10
Orellena	1.978.956,09	Cotopaxi	182.580,51
Sucumbíos	1.586.171,62	Chimborazo	111.567,76
El Oro	1.245.928,92	Loja	76.420,67
Morona Santiago	736.292,89	Galápagos	54.768,39
Pichincha	684.742,44	Bolívar	42.287,72
Imbabura	538.415,28	Carchi	22.700,12
Esmeraldas	451.604,07	Zamora Chinchipe	18.122,89
Manabí	353.477,46		

The main hydroelectric power plants are located in these three provinces. Tungurahua hosts the hydroelectric plants: San Francisco, Agoyan, Topo and Pucará. The participation of this sector is overwhelming. The San Francisco hydroelectric power plant with a production of 1221.89 [GWh] is of interest for the present work [1].

1.2 Erosion mechanisms

Erosion is the wear caused by sediment-laden water in turbomachinery. This is a general definition and it varies according to the author [11].

Wear is the destruction and progressive loss of the material of an element due to an interaction between components or substances. Erosion wear is caused by the impact of solid or liquid particles on a solid surface. The impacting particles have sufficient kinetic energy to damage metallic surfaces [11].

Turbomachinery in hydropower plants suffer serious damage from erosion. Francis turbine runners, guide vanes and other components are eroded by sediment laden water. Hydropower plants operate at different points according to environmental conditions, which aggravates erosion damage [11].

- Cutting

Occurs when sharp-edged particles hit the surface with a low angle impingement and remove the material, as shown in figure 1.2. Sharp edges remove material by scrubbing or scraping the metallic surface forming short track-length scars [11, 12].

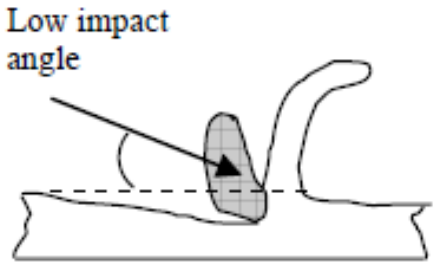

Figure 1.2: Cutting erosion (Source: [11])

- Plastic deformation

  Plastic deformation occurs by repeated strikes of the particles with medium speed and large impingement angle on the flakes, as shown in figure 1.3. Flakes are formed around an impact point, they are detached as debris[11, 12].

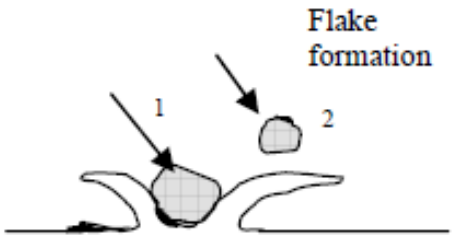

Figure 1.3: Plastic deformation erosion (Source:[11])

- Fatigue

  Fatigue occurs due to the repetitive impact of the particles at low speed and with a large angle of impact on the surface, as shown in figure 1.4. The surface weakens and cracks are generated. This causes detachment of material from the surface [11, 12].

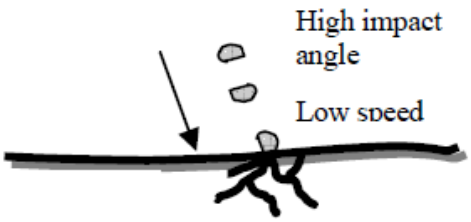

Figure 1.4: Fatigue erosion(Source: [11])

- Brittle fracture

  It occurs when the particles hit fragile surfaces at medium speed and large impact angle. The surface is fragmented and there is detachment of the material, as shown in figure 1.5. Fragmentation occurs by subsurface cracking [11, 12].

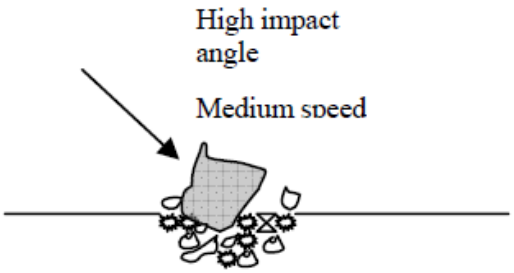

Figure 1.5: Brittle fracture erosion (Source:[11])

1.3 Approaches two phases flow modelling

Liquid-solid flow can be modeled taking two approaches into account:

- Eulerian-Eulerian
- Eulerian-Lagrangian

Eulerian-Eulerian

This approach treats the two phases as continuous phases. The local turbulence field of continuous phases governs transport properties. The movement of the flow is adjusted to the particularity established in a specific location in space and time. Each material is

assumed to occupy the same volume in space. The mass and moment equation is established in terms of moment exchange for each phase[50]. The figure 1.6 shows this approach.

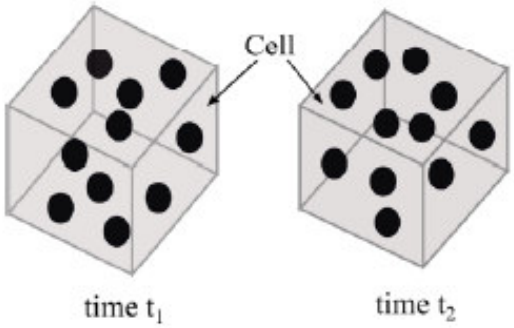

Figure 1.6: Eulerian-Eulerian approach (Source:[50])

Eulerian-Lagrangian

Eulerian-Lagrangian approach treats the continuous phase by the Eulerian method and the movements of the dispersed phases is treated by the Lagrangian method.The solution of the dispersed phase is calculated based on the solution of the continuous phase. The continuous phase is modeled as monophasic. For this, a parcel of particles is considered as a single particle. with the same properties. The observer follows them through space and time. The properties are calculated based on the change of the properties in the follow-up [51], as can be seen in the figure 1.7.

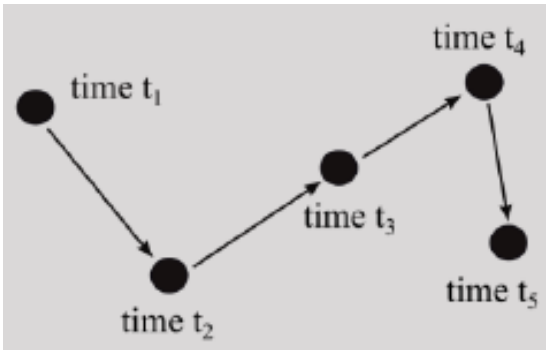

Figure 1.7: Eulerian-Lagrangian approach (Source:[51])

1.3.1 Parametric models

Various erosive wear models for turbomachines can be found in the literature. Some of them are listed below.

Naidu [52] presents his erosion model. Where sediment erosion rate is defined by:

$$E(mm/year) = C * K_{hd} * K_{sz} * K_{sh} * K_{mt} * V_r^n \tag{1.1}$$

Where:
C: sediment concentration coefficient
K_{hd}: hardness coefficient
K_{sz}: size coefficient
K_{sh}: shape coefficient
K_{mt}: wear coefficient of the material
V_r: relative velocity of water and sediment particles with respect to the runner.

n takes values depending on the element: for Francis runner turbine $n = 3$, for Francis guide vanes turbines $n = 2.5$, for Pelton nozzle $n = 1.5$, for Pelton runner buckets $n = 1.5$.

Padhy [53,54]in his work shows a correlation in the loss of efficiency in turbomachines as a function of K_{sz}, C, V and t. Erosive wear rate is shown in the following expression:

$$E = 4.02x10^{-12} * K_{sz}^{0.0567} * C^{1.2267} * V^{3.79} * t \tag{1.2}$$

Where:
K_{sz}: particle size factor
C: sediment concentration
V: jet velocity
t: operating hours

This model is developed based on experimental data collected for different operating conditions.

Tsuguo [55] in his work performs data collection of 18 hydropower plants for the time of 8 years. He shows the correlation of factors based on the data collected. Erosion rate is expressed with the following equation:

$$E(mm/year) = \beta * C^x * K_{sz}^y * K_{sh} * K_{hd} * K_{mt} * V_r^n \tag{1.3}$$

Where:
β: turbine coefficient at eroded part
C: concentration of suspendent sediments
V_r relative velocity of two phase flow with respect to runner
x: exponent value for concentration
y: exponent value for size
n: exponent value for velocity, for Pelton turbine $n = 1.5$, for Francis runner $n = 2.5$

International Electrotechnical Commission (IEC) [55] recommends using the following expression to determine the depth of abrasion:

$$E = W^{3,4} * PL * K_{mt} * \frac{K_{fl}}{RS^p} \tag{1.4}$$

Where:
PL: particle load integrated over time
W: velocity characteristic
k_{fl}: constant for each turbine component provided for impingement angle and flow turbulence
RS: Reference turbine diameter
p: exponent for each turbine component
K_{mt}: material constant

Some erosive wear models for turbomachines have been mentioned. These are applicable for Francis and Pelton turbines with acceptable results [57].

1.4 State of art

Koirala [8] in his study on erosion of Francis turbine guide vanes shows that the erosion of these elements is crucial to have a high performance in sediment laden waters. Slow sediment impacts initiate erosion leading edge, trailing edge and clearance gap. Cross flows, leakage flows and friction losses are amplified. It is shown that the estimation of erosion is necessary to mitigate this phenomenon and its consequences.

Thapa [9] in his work on sediment erosion and its effects on guide vanes in Francis turbines shows that instabilities in the flow originate in the guide vanes, also the erosion in the guide vanes contributes to the increase of the clearance gap. The effects of erosion on the guide vanes directly affect the power production of the Francis turbine and reduce its efficiency.

Acharya [10] carried out a numerical study on sediment erosion in the guides vanes of a Francis turbine. He predicts the erosion pattern of in these components. He identifies the most affected areas in the element which allows future work to improve the designs of the guide vanes profiles and runner blades.

Koirala [5] in his experimental and numerical work selects a NACA profile for a Francis turbine's guide vane. The NACA profiles studied are: 0012, 1412, 2412 and 4412, as shown in figure 1.8. The NACA 4412 shows the best performance. Erosion in NACA 4412 is the

lowest in comparison with the other profiles and pressure difference between SS and PS is the lowest. The asymmetric profile has the best behavior for the case study.

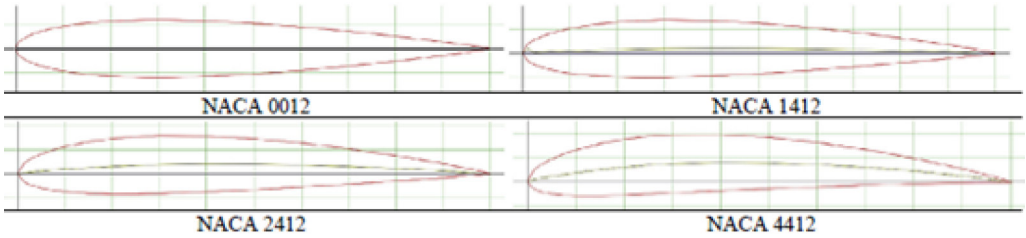

Figure 1.8: Guide vanes profiles NACA (Source:[5])

Lama [6] in his work, performs a numerical analysis of the performance of the Francis turbine runner with different guide vanes profiles. The study concludes that the NACA profile 4412 and 2412 compared to the NACA 0012 show better efficiency in all operating ranges, as shown in figure 1.9. NACA profile 4412 shows the best performance and the least erosion on the runner blades.

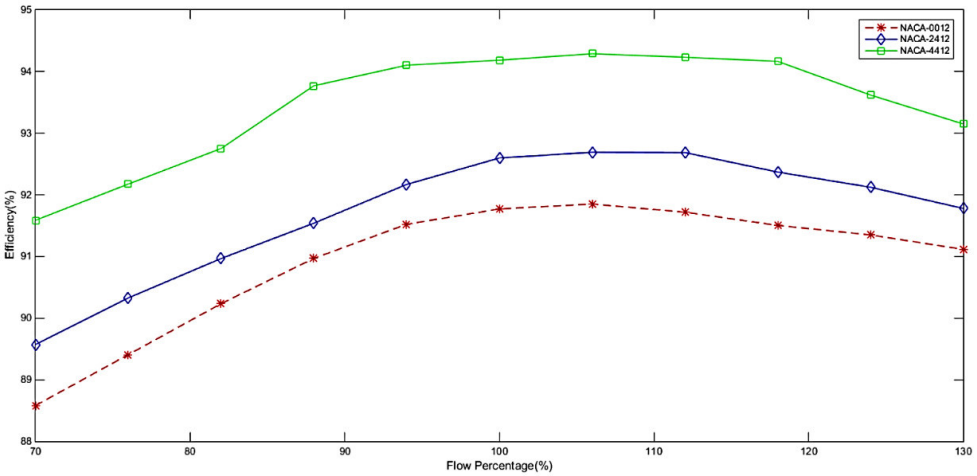

Figure 1.9: Efficiency (Source: [6])

Chitrakar [4] in his work performs a numerical analysis of the guide vanes on the performance of Francis turbines. He uses different NACA profiles concluding that that if the NACA profile 4412 is used the pressure difference between adjacent sides is reduced. Runner efficiency is increased with the NACA profile 4412 compared to the NACA profile 0012 for all operating points. The pressure pulsation in the runner's inlet is reduced around 60% with tne NACA profile 4412 at the BEP. The improvements are noticeablein guide

vanes with asymmetrical profiles.

Nora [7] in his master's thesis, studies the erosion caused by sediments in guide vanes numerically and experimentally. She shows that the NACA profile 4412 is the best for reducing erosion in guide vanes for the Francis turbine.

Yánez (2017), in his thesis on parametric design of runner blades. Applies the Gjøsæter design model [48] to obtain the preliminary model programmatically in Matlab. He the performs analysis in CFD where he manages to visualize qualitatively the erosion of its design. However, these effects are barely visible and therefore require a more detailed study [47].

Bone (2017) in his master's thesis on the parametric design methodology for Francis turbines with multiobjective optimization through the application of genetic algorithms manages to obtain a design of the runner blades that decreases the erosion tendency consequently reducing erosion considerably. He checks his result in ANSYS CFX concluding that it is possible to innovate the design of turbine components [16].

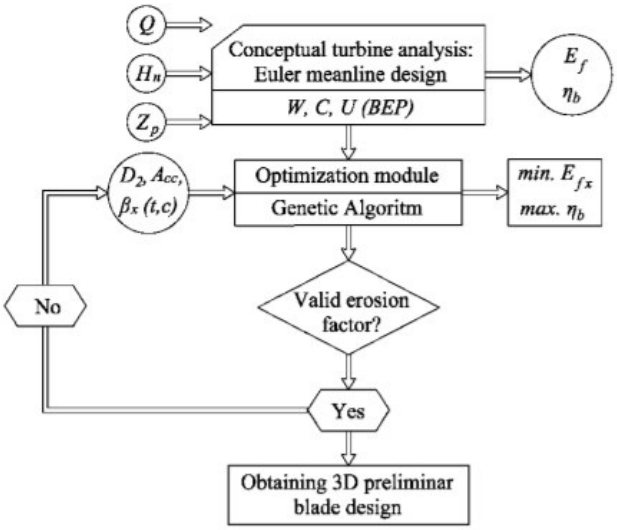

Figure 1.10: Design process (Source: [16])

Biraj Thapa [15] explains procedures for the design of high head Francis turbines. He explains the effects on sediment erosion on the runner. The design parameters such as reduced peripheral speed at the inlet, height of the runner, among others, are varied and the effects on the erosion factor are evaluated. He establishes two terms as indicators of

erosion in the runner, the erosion tendency (E_t) and the erosion factor (E_f). The results of the erosion factor are compared with the results of the numerical analysis by using CFD codes for the proposed design. To obtain the results he uses the Jhimruk hydropower plant in Nepal as a reference case study.

Chapter 2

METHODOLOGY

Two approaches are considered for the design of the guide vanes.

- Quasi-two dimensional approach

  An analysis is carried out taking into account a quasi two-dimensional approach. A methodology is followed that allows selecting a NACA profile. Drag and erosion are analyzed with dimensionless numbers. There are input parameters such as Discharge and Head and the results are the speed triangles at the runner inlet. The NACA profiles are selected for the guide vanes the sediment erosion is analyzed using dimensionless numbers.

- High fidelity design

  An analysis is carried out using commercial CFD codes of the proposed design. Computationals tools are used for a high fidelity design. The numerical methods that allow you to analyze the two phase flow are described. For the turbulence modeling the k-omega SST model is implemented. Finnie erosion model is used to predict wear.

2.1 Analysis using a quasi-two dimensional approach

The analysis consists of 3 sections:

- Parametric modeling.
- Dimensionless analysis.
- Erosion analysis.

Figure 2.1 shows the diagram of the proposed methodology to select the appropriate profile for the guide vane to reduce the sediment erosion in the runner blades. The methodology considers a direct relation between the erosion on the runner and relative flow velocity. First, the Flow Rate (Q_d) and Net Head (H_d) are considered as inputs for a parametric modelling. Based on Euler meanline design, six parameters are chosen: inlet diameter, outlet diameter, degree of reaction, inlet reduced peripheral velocity, flow acceleration and the blade angle distribution, for the parametric modelling. The design for the best efficiency point(BEP) was carried out, where the following parameters are calculated: relative flow velocity (W), Peripheral velocity (U), absolute velocity (C) and and the exit angle (α_0). Based on these results, a non-dimensional analysis was done for NACA profiles. The drag coefficient was analysed for different attack angles using the software JavaFoil. The profiles which generates the minimum drag was selected. Then, the velocity triangles at inlet and outlet of the runner in the best efficiency point (BEP) are determined. After completing the described steps, the velocity triangle was analyzed. changes in the direction of the fluid at the exit of the guide vane were checked the fluid speed at the exit of the guide vane (runner relative velocity inlet). Afterwards, the Erosion Tendency (E_t) and the Erosion Factor(E_f) (shown in equations 2.16 and 2.17) were calculated using the models proposed by Biraj Thapa [15]. These factors are used to analyze the reduction of the erosion in the runner. The erosion factors are compared and the profile that presented the lowest is selected.

2.1.1 Parametric modelling

Input parameters

The design of a hydropower plant depends on various parameters and requirements. Euler's approach is taken into account for the parametric design of the guide vanes. Two parameters are taken into account as a starting point for the design: head and discharge [13, 14].

- **Discharge**

  Specific design discharge is necessary for the design of the turbomachine. During the operation of the hydropower plant it should have an optimal and profitable energy production. The turbine design discharge is determined by setting the number of Q_d [13, 14].

- **Head**

  Net head of the system is required. Then, the design head value is determined as the difference in energy between the inlet and outlet of the turbomachine. The value of

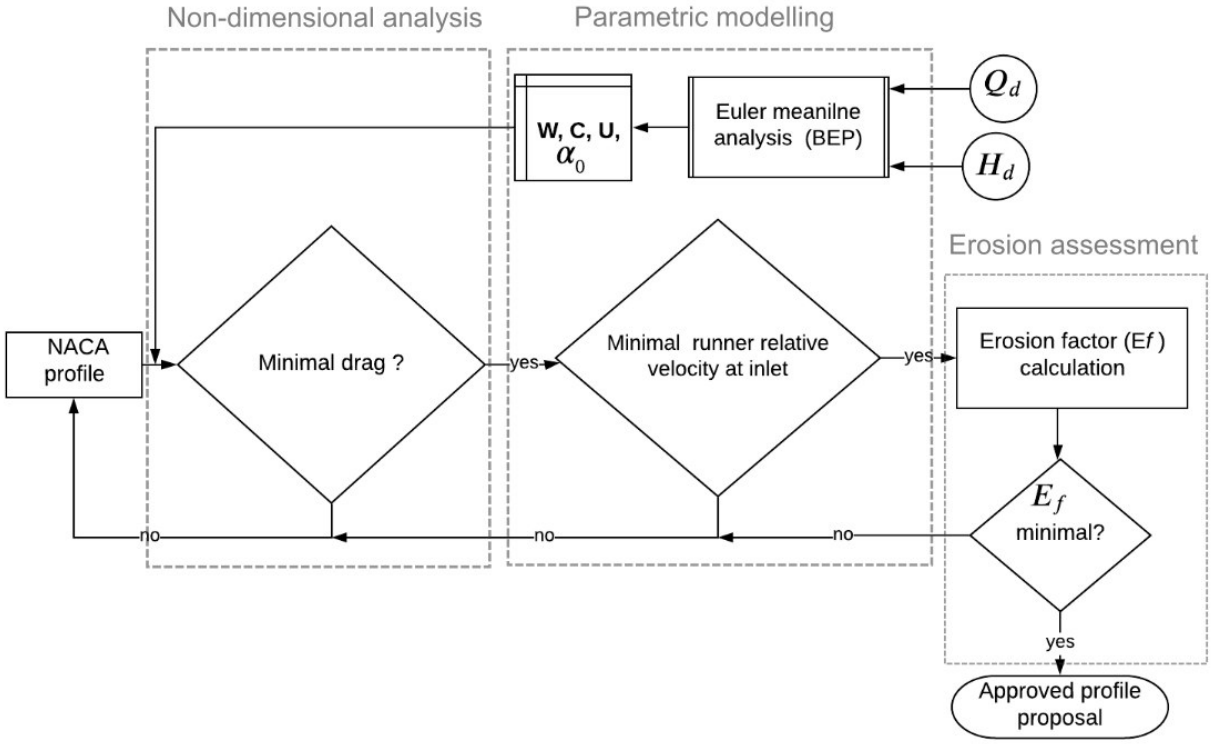

Figure 2.1: Selection methodology chart (Source: Own)

H_d is obtained from equation 2.1 [13, 14].

$$H_d = H_s - H_L \tag{2.1}$$

Where
H_s: gross static head, difference between the head water elevation and tail water elevation
H_L: head loss term including hydraulic losses in the conduits

2.1.2 Design parameters

Power

The total hydraulic power available to the turbine (P) is calculated with equation 2.2 from the net head.

$$P_d = \rho g Q_d H_d \tag{2.2}$$

Where:

- g: gravitational aceleration [m^3/s]
- Q_d: design discharge [m^3/s]
- H_d: design head [m]

Rotational Speed

Power and design head allow to calculate the rotational speed of the runner, with equation 2.3, as a preliminary value.

$$n = n_q \frac{H_d^{1.25}}{P_d^{0.5}} \tag{2.3}$$

$$n_q = \frac{c_{nq}}{H_d^{0.535}} \tag{2.4}$$

$$c_{nq} = min(2600; 2600 - (200000 - P_d)/365) \tag{2.5}$$

Where n is in rpm; Pd is the power in KW; nq is the specific speed of the runner. The generator must work at synchronous speed depending on the number of poles, 22, and the frequency 60Hz for the case study.

$$n_{sync} = \frac{120f}{2(numberofpoles)} \tag{2.6}$$

2.1.3 Guide vanes

Guide vanes (GV) direct fluid to the runner inlet. GV regulates the flow of the fluid. This element has an axis of rotation which must not disturb the flow of the fluid towards the runner inlet. D_g is the diameter of the circle that passes through the center of rotation of the guide vanes. D_g is equal to 1.6 of the diameter of the runner inlet D1 according to equation 2.7. For the case study the number of guide vanes is 20.

$$D_g = 1.16 D_1 \tag{2.7}$$

$$L_g = \frac{\pi D_g}{number of guide vanes * 0.9} \tag{2.8}$$

The length of the hydrofoil is calculated according to equation 2.8. The GV axle spacing is calculated according to Equation 2.9. The initial axis diameter of the GV is determined with equation 2.10.

$$t_g \approx \frac{D_g \pi}{number of guide vanes} \tag{2.9}$$

Calculate the initial axis diameter The diameter of the GV inlet is calculated from the cosine theorem with equation 2.11, once the outlet diameter, its shaft diameter and its length are already known.

$$D_{axf} = D_1 * (0.29 * \Omega^* + 1.07) \tag{2.10}$$

$$D_{gvi} = 2 * \sqrt{L_{gv}^2 + \frac{{D_{gvo}}^2}{4} - 2L_{gv}\frac{D_{gvo}}{2} * \cos(\frac{\pi}{2} - \alpha_0)} \tag{2.11}$$

2.1.4 Turbine working principle

GV outlet creates a circulation of water around the axis of the turbine. the circulation of the fluid is defined by equation 2.12.

$$\Gamma = \oint_c V.dl \tag{2.12}$$

Where:
Γ: is the circulation
V: is the flow velocity vector
C: is a closed curve in the flow field
dl: is the differential line of segment of the closed curve C

The above equation can be written as its dot product

$$\Gamma = \oint_c V \cos(\alpha) dl \tag{2.13}$$

Where:
α is the angle between the velocity vector and the differential line vector

The equation 2.13 can be expressed as:

$$\Gamma_0 = (\pi D_0) v_0 \cos(\alpha_0) \tag{2.14}$$

Where:
Γ_0: is the circulation at the GV outlet
D_0: is the outlet diameter of GV
v_0: is the average flow velocity at the GV outlet
α_0: is the flow angle in the tangential direction

2.2 Dimensionless number analysis

2.2.1 Drag forces

The drag forces that are generated in the different elements of the Francis turbine are undesirable. Therefore, a non-dimensional analysis is performed. First, the focus is on the variation of the drag coefficient (C_D). The energy losses that could occur are verified. In two-dimensional form, the GV profiles are analyzed. Equation 2.15 describes the variation of the C_D for the different NACA profiles. Different angles of attack are considered taking as a start and reference the zero (0) degree angle.

$$\Delta C_D = \frac{C_{Di-1} - C_{Di}}{C_{Di-1}} \tag{2.15}$$

Where:
ΔC_D is multiplied by 100 to obtain the percentage variation C_{Di} is the drag coefficient for an angle of attack α_i.
The coefficient at the current position is subtracted from the value of the previous position. The difference obtained is divided for the the previous value.

2.2.2 Erosion estimation

Erosion Tendency and the Erosion Factor by Thapa [15] and Bone [16] were calculated, based on the variations of the relative velocity in the runner. For that, the velocity triangles were analyzed at the BEP condition. The following equations were used to the estimation:

$$E_t = \frac{\sum W_i^3 A_i}{\sum A_i} \tag{2.16}$$

W_i is the relative velocity in each segment area Ai on the runner blade.

$$E_f = \frac{(E_t)_{newdesign}}{(E_t)_{referencedesign}} \tag{2.17}$$

$$E_t = \frac{W_1^3 C_{m2} + W_2^3 C_{m1}}{C_{m1} + C_{m2}} \tag{2.18}$$

The sub-indices indicate the speeds at the runner's inlet and outlet.

2.3 High fidelity design based on computational fluid mechanics

2.3.1 Numerical models for predicting two phase flow

Liquid modeling

The equations that govern the flow of liquids are those of mass and momentum conservation. The conditions and assumptions necessary for flow prediction are described [21]. Continuity conservation is presented with the following expression in a Eulerian formulation:

$$\frac{\rho\partial\left(\theta_l\right)}{\partial t}+\frac{\rho\partial\left(\theta_l u_i\right)}{\partial x_i}=S_m \tag{2.19}$$

Where:
i, j: space axes subscripts
S_m: mass exchange between phases, for liquid-solid flow $S_m = 0$
u : continuous phase velocity
θ_1: liquid phase volume fraction
ρ: continuous phase density
t: time

The equation for the conservation of momentum is expressed below:

$$\frac{\rho\partial\left(\theta_l u_i\right)}{\partial t}+\frac{\rho\partial\left(u_i u_j\right)}{\partial x_j}=-\frac{\partial p}{\partial x_i}+\frac{\partial}{\partial x_j}\left[\mu\left(\frac{\partial u_i}{\partial x_j}+\frac{\partial u_j}{\partial x_i}\right)\right]+S_{p\varphi,i'} \tag{2.20}$$

Where:
p: pressure
μ: dynamic viscosity
$S_{p\varphi,i}$: moment produced in the fluid by the action of the particle

On the right hand is the interphase exchange momentum. This represents the momentum transfer between phases, this transfer will be different according to the approach [22].

This model has been validated by several researchers, the model does not consider the volume for the solid phase [23,24].

Solid numerical modeling

When using the Lagrangian approach to model the solid particles to predict erosion, the following assumptions are considered [6,41,48]:

- The size of the particles is smaller compared to the cell volume dimension.
- The particle is spherical
- Interaction between particles is not considered.
- The physical properties of the solid phase are considered constant.
- Brownian motion of the particles and their rotation are not considered.

The discrete phase model is applied to calculate the trajectory and velocity for each particle according to Newton's second law as expressed in equation 1.3:

$$\frac{\partial \left(v_p\right)_i}{\partial t} = F_{Di} + F_{pi} + F_{Bi} + F_{mi} + F_{others} \tag{2.21}$$

Where:
v_p: particle velocity
F_D: drag
F_p: pressure gradient
F_B: buoyancy
F_m: virtual mass force and lift force
F_{others}: others forces

Drag force

Viscous stresses and unbalanced pressure distribution between solid particles and fluids result in drag force. When considering the particle as a sphere, the drag force can be expressed with equation 1.4 [28].

$$F_{Di} = \frac{\mu}{\rho_p d_p^2}.\frac{18.C_D.Re}{24}\left(u_i - v_{pi}\right) \tag{2.22}$$

Where:
ρ_p: particle density
d_p: particle diameter
C_D: drag coefficient
Re: Reynolds number
The drag coefficient is given by:

$$C_D = \frac{f_{drag}Re}{24} \tag{2.23}$$

$$\mathrm{f}_{drag} = \left\{ \begin{array}{ll} 1 + 0.15Re^{0.687} & Re \leq 1000 \\ 0.01883\mathrm{Re} & \mathrm{Re} > 1000 \end{array} \right\}$$

Pressure gradient force

The pressure gradient is the force on the particle in the direction of the pressure gradient of the fluid. The following equation allows its calculation [29]:

$$F_{pi} = \left(\frac{\rho}{\rho_p}\right)\left(v_p\right)_i \frac{\partial u_i}{\partial x_i} \tag{2.24}$$

Buoyancy force

The buoyancy force according to Archimedes' principle is equal to the weight of the displaced fluid [23]. This force is given by:

$$F_{Bi} = \left(1 - \frac{\rho}{\rho_p}\right) g \tag{2.25}$$

Virtual mass force

Virtual mass force is the force necessary for the movement of the particle in the continuous phase. The fluid accelerates along with the particle. This is represented by the following expression [30]: $Itisthe forcenecessary forthemovementofthe particleinrelationtothecontinuousphas$

$$F_{mi} = -\frac{1}{2}\frac{\rho}{\rho_p}\frac{\partial}{\partial t}\left(u_i - v_{pi}\right) \tag{2.26}$$

Other forces

Different forces are considered depending on the case study [22,31]:
The rotational force is considered, that is, the sum of coriolis and centripetal forces.

Brownian diffusion forces consider the random movement of particles as they move from a low-concentration flow to a high-concentration flow.

The lifting force is given by shear perpendicular to the direction of flow experienced by the particle in a field of shear flow.

Wall interaction

When the particle hits a wall, it loses energy, the reflected velocity is reduced compared to the incident velocity. The loss of energy is expressed by coefficients of restitution that

relate the velocity of impact and the reflected velocity. This is expressed with the following equations [22]:

$$e_n = \frac{v_n^r}{v_n^i} \tag{2.27}$$

$$e_t = \frac{v_t^r}{v_t^i} \tag{2.28}$$

Where:
e_n:normal restitution coefficient
e_t:tangential restitution coefficient
v_n^r:normal component of the reflected particle velocity

v_t^r : tangential component of the reflected particle velocity
v_n^i: normal component of the incident particle velocity
v_t^i: tangential component of the incident particle velocity

2.3.2 Interaction between phases

Eulerian Lagrangian approach in the interaction between the phases will depend on the concentration and the size of the particles, also on the smallest simulation scale [32,33,34].

Momentum interaction

As a point source, the effect of the particle in the flow of the liquid phase is considered. If the particle is smaller than the Kolmogorov length scale, the effect is calculated using the following expression:

$$\eta = \left(\frac{\upsilon^3}{\varepsilon}\right)^{\frac{1}{3}} \tag{2.29}$$

Where:
ε: energy dissipation rate
υ: kinematic viscosity of the fluid

If the particle is equal to or greater than the smallest turbulence scale, the contribution of the boundary layers generated on the surfaces of the particles to the fluid dynamics must be included. Shuen et al. [35] proposes the following expression for the calculation

of the moment source term produced by the presence of the particle in the continuous flow

$$S_{p\varphi,i} = \frac{1}{V}\sum_{n=1}^{N_T} \dot{n}_i m_p \left[\left(v_p\right)_{\frac{i}{in}} - \left(v_p\right)_{\frac{i}{out}} \right] \tag{2.30}$$

Where:
V: volume cell $\dot{n}_i$: number of particles per unit time in each group
N_T: all trajectories that traverse a computational cell
$\left(v_p\right)_{\frac{i}{in}}$: particle velocity at the inlet of the cell
$\left(v_p\right)_{\frac{i}{out}}$: particle velocity at the outlet of the cell

2.3.3 Turbulence modelling

There are several models of turbulence such as k-epsilon, SAS, DES, LES among others. The use of the models depends on the application. In the present work, the RANS Standard k-ω-SST model is implemented, which according to several authors is the most suitable for Francis turbines.

RANS Standard k-ω SST

The standard k- ω SST model is an empirical model based on model transport equations for the turbulent kinetic energy (k) according to the equation 1.14 and the specific (ω) dissipation rate according to the equation 1.15

$$\frac{\partial(\rho k)}{\partial t} + \frac{\partial(\rho k u_i)}{\partial x_i} = \frac{\partial}{\partial x_j}\left(\Gamma \frac{\partial k}{\partial x_j}\right) + G_k - Y_k + S_k \tag{2.31}$$

$$\frac{\partial(\rho \omega)}{\partial t} + \frac{\partial(\rho \omega u_i)}{\partial x_i} = \frac{\partial}{\partial x_j}\left(\Gamma \frac{\partial \omega}{\partial x_j}\right) + G_\omega - Y_\omega + S_\omega \tag{2.32}$$

Where G_k is the generation of turbulent kinectic energy due to mean velocity gradients. G_ω is the generation of ω. Γ_k and Γ_ω are the effective diffusivity of k and ω. Y_K and Y_ω are the dissipation of k and ω due to turbulence.

Modelling the Effective diffusivity

$$\Gamma_k = \mu + \frac{\mu_t}{\sigma_k} \tag{2.33}$$

$$\Gamma_\omega = \mu + \frac{\mu_t}{\sigma_\omega} \tag{2.34}$$

Where σ_k and σ_ω are the turbulent Prandtl numbers. Turbulent viscosity μ_t is calculated as follows:

$$\mu = \alpha^* \frac{\rho k}{\omega} \tag{2.35}$$

Low-Reynolds-Number Correction

Coefficient α^* damps the turbulent viscosity causing a low-Reynolds-number correction. The expression 1.19 shows this parameter.

$$\alpha^* = \alpha^*_\infty \left(\frac{\alpha^*_0 + Re_t/R_k}{1 + Re_t/R_k} \right) \tag{2.36}$$

Where:

$$Re_t = \frac{\rho k}{\mu \omega}$$

$$R_k = 6$$

$$\alpha^*_0 = \frac{\beta_i}{3}$$

$$\beta_i = 0.072$$

For high Reynolds number $\alpha^* = \alpha^*_\infty = 1$

Turbulence modulation

It is possible that the level of turbulence is altered if there is presence of solid particles [38,39,40], that is why it should be analyzed when it should be considered or not. Elghobashi [36] shows a diagram of the effect of particles on continuous phase turbulence based on solid particle volume concentration Cv and particle response time τ_R.

If the particles have $C_v < 10^{-6}$ the type of coupling is One way, that is, turbulence is not affected.

If the particles have $10^{-6} < C_v < 10^{-3}$ the type of coupling is Two way, that is, the turbulence of the liquid phase is disturbed. If the particles attenuate the turbulence $\tau_R < 1$.

If the particles increase the turbulence $\tau_R > 1$.

If the particles have $C_v > 10^{-3}$ the type of coupling is Four way, that is, the collision and the presence of solid particles modify the turbulence [37,38,39].

2.3.4 Erosion models

There are several empirical and other numerical models. Some of those models are detailed below. For the present work, Finnie's model is used since it has been implemented in numerous works.

Finnie Model

Finnie's model of erosive wear relates the kinetic energy of impact on the walls to the rate of wear[19].

$$E = kV_p^n f(\gamma) \tag{2.37}$$

Where:
E: dimensionless erosion mass
k: model constant
V_p: particle impact velocity
$f(\gamma)$: dimensionless function of the impact angle γ

n: for metals it is generally in the range 2.3 to 2.5 [rad].

This relationship between wall impact and kinetic energy is represented by the following function:

$$f(\gamma) = \frac{1}{3} cos^2\gamma \quad \text{for} \quad \gamma > 18.5^\circ \tag{2.38}$$

$$f(\gamma) = sin2\gamma - 3sin^2\gamma \quad \text{for} \quad \gamma \leq 18.5^\circ \tag{2.39}$$

McLaury erosion model

McLaury erosion rate (E) is defined by equation 1.2. McLaury erosion model is for predicting erosion by sand particles in water [18].

$$E = AV^n f(\gamma) \tag{2.40}$$

$$A = FBh^k \tag{2.41}$$

Where:
F: empirical constant
V: particle impact velocity
Bh: Brinell's hardness number of wall material
k: -0.59 for carbon steel. For other materials it is different
with

$$f(\gamma) = b\gamma^2 + c\gamma \quad \text{for} \quad \gamma \leq \gamma_{lim} \tag{2.42}$$

Where:
b,c,w,x and y: model constant, must be determined by an experiment
z: must be chosen in such a way that the angle functions when $\gamma = \gamma_{lim}$
γ_{lim}: transition angle [18]

Oka erosion model

E is the Oka erosion rate[20]. E is defined by the equation:

$$E = E_{90} \left(\frac{V}{V_{ref}}\right)^{k2} \left(\frac{d}{d_{ref}}\right)^{k3} f(\gamma) \tag{2.43}$$

Where:
E_{90}: reference erosion ratio at 90°impact angle
V: particle impact velocity
V_{ref}: reference velocity
$k2$ and $k3$: velocity exponent and diameter exponent
$f(\gamma)$: impact angle function

The impact angle function depends on the erosion as:

$$f(\gamma) = (sin\gamma)^{n1}(1 + H_v(1 - sin\gamma))^{n2} \tag{2.44}$$

Where:
γ: wall impact angle (rad)
H_v : wall material vickers hardness(GPa)
n_1 and n_2: angle function constants

2.3.5 Computational domain

The computational domain is established according to the case study. Figure 2.2a shows the configuration of the turbomachine: stay vane, guide vane and runner vane.

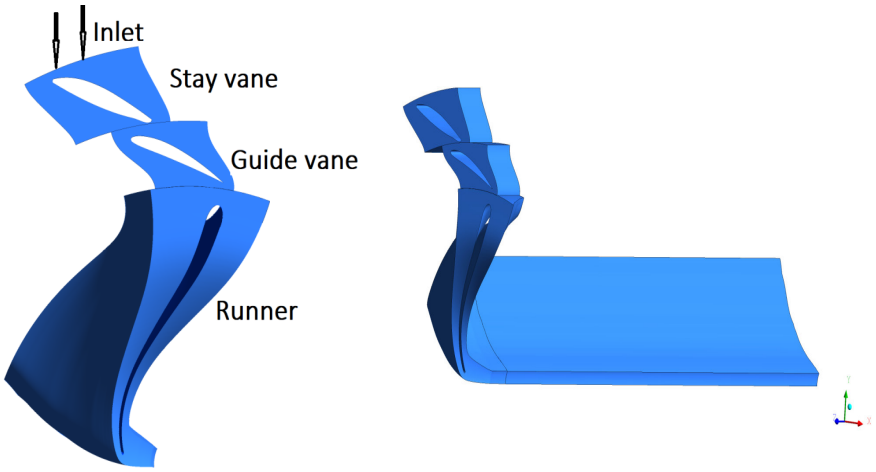

(a) (b)

Figure 2.2: Computational domain (Source: Own)

2.3.6 Mesh generation

The mesh of the computational domain is generated using commercial software.

The figure 2.2b shows the geometry configuration. Meshing is done with the TutboGrid software, setting is shown in table 2.1.

The figure 2.3 shows the post-process result for the stay vane, guide vane and runner vane.

Table 2.1: Setting TurboGrid

Setting	
Details of mesh data	
Method	Target Passage Mesh Size
Node Count	Coarse, Medium and Fine
Boundary Layer Refinement Control	
Method	Edge refinement factor
Factor	5
Near Wall Element Size Specification	
Method	y_+
Reynolds No.	1e9

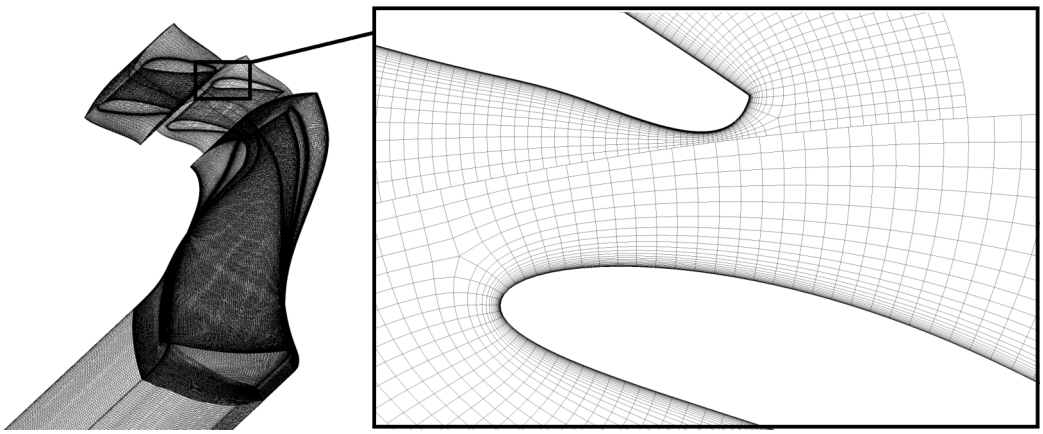

Figure 2.3: Structured mesh (Source: Own)

Continuity conservation is verified. Table 2.2 shows the results where it is verified that the error is below 1%. Therefore, the results obtained are reliable.

Table 2.2: Continuity conservation

Configuration	Continuity conservation [kg/s]	% error
NACA 0012	-0.6497852	-0.022%
NACA 4412	-0.6676294	-0.023%
NACA 5412	-11.12989	-0.384%
NACA 6412	-11.1555	-0.385%

y^+ is obtained with the equation 2.45.

$$y^+ = \frac{u_\tau y}{\nu} \tag{2.45}$$

Where:
u_τ: friction velocity
y: distance to the nearest wall
ν : kinematic viscocity

The calculated values of y^+ are between the values of 7.868697 and 18.098627 as can be seen in the figure 2.4, which are adequate the model used k-omega SST.

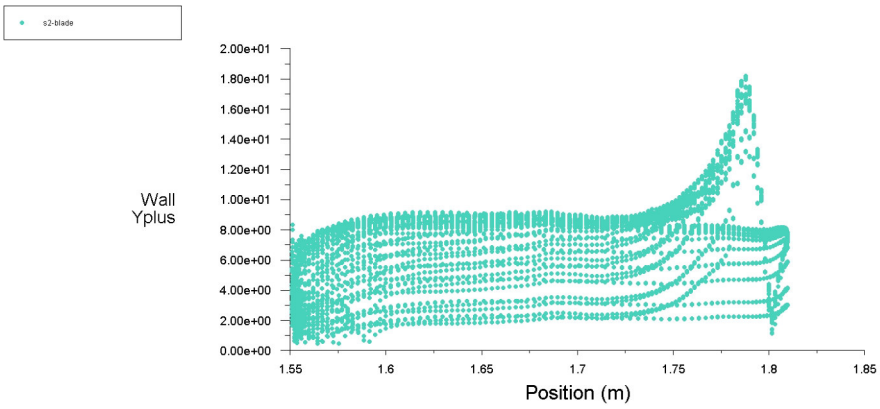

Figure 2.4: y_+ guide vanes (Source: Own)

Mesh independence

Mesh independence for the **k-ω SST** model is performed for each profile under analysis as shown in the table 2.3, 2.4, 2.5 and 2.6, where the pressure drop between the inlet and outlet domain is verified. Three mesh solutions are tested with a difference in the number of nodes in the guide vane section where a minimal variation of $\triangle$ P is observed, as shown in figure 2.5 . The case with the number of Medium nodes is selected for each case.

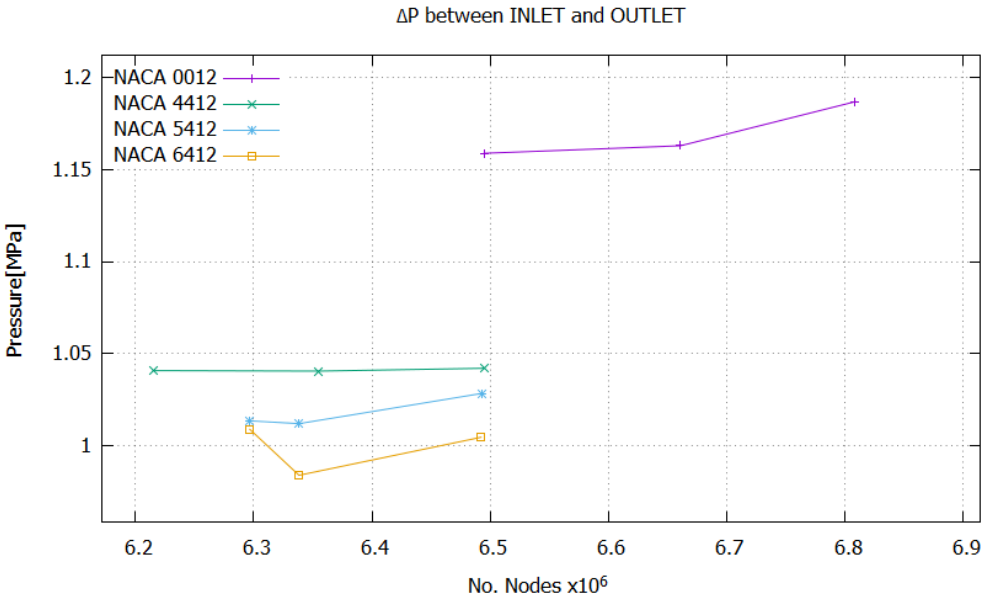

Figure 2.5: Mesh validation, $\triangle P$ (Source: Own)

Table 2.3: NACA 0012

Mesh	Nodes	$\triangle P[Pa]$
Coarse	6494802	1158961
Medium	6660969	1163086
Fine	6808673	1187020

Table 2.4: NACA 4412

Mesh	Nodes	$\triangle P[Pa]$
Coarse	6214922	1040857
Medium	6355046	1040578
Fine	6495170	1042119

Table 2.5: NACA 5412

Mesh	Nodes	$\triangle P[Pa]$
Coarse	6296744	1013558
Medium	6338302	1012053
Fine	6493434	1028556

Table 2.6: NACA 6412

Mesh	Nodes	$\triangle P[Pa]$
Coarse	6296744	1008942
Medium	6338302	984005.6
Fine	6492256	1004654

2.3.7 Solver setting

ANSYS Fluent 2018 commercial tool was used to solve the equations. The **Shear-Stress Transport (SST) k-ω model** is implemented through defined functions. The table 2.7 shows the configurations made. The solution method for the liquid phase is the SIMPLE.Inlet of stay vanes and non-overlapping interfaces of the runner are assigned as TOTAL MASS FLOW INLET. Stay vane and guide vane are assigned as stationary, the runner is configured as ROTATING FRAME. PERIODIC REPEATS INTERFACES are created between stay vanes and guide vane, runner and outlet interfaces. Then, between the runner and guide vane to STANDARD INTERFACE is assigned. Finally, the nonslip condition is assigned for the walls. For the Solid Phase, Discrete phase model is activated.

Table 2.7: Solver setting

Setting	
General	
Precision	Double precision
Solver type	Pressure-based
Time	Steady
Solution method	
Pressure-velocity coupling	SIMPLE
Spatial discretization	*Gradient*: Least Squares Cell Based
	Pressure: Second order
	Momentum, Turbulent Kinetic Energy
	and Specific Dissipation Rate:
	Second Order Upwind
Solid phase model	Discrete phase model
Interaction	Interaction with continuous phase
Model configuration	Max. numbers of steps = 350000
	Specify length scale=1x10^{-5}
	Physical models: Saffman Lift Force, Virtual Mass Force
	Pressure Gradient Force, Erosion/accretion
Numerics	*Tracking Scheme*: Automated
	High order Scheme: Trapezoidal
	Low order Scheme: Implicit

2.3.8 Boundary conditions

Table 2.8 details the boundary conditions for the two solid and liquid phases for the domain shown in figure 2.2. The data are obtained from the company CELEC E.P. [42].

Table 2.8: Boundary conditions

Boundary condition	Inlet
Liquid phase	
Mass flow	2900 [kg s^{-1}]
Pressure	2093454 [Pa]
Turbulent intensity	5%
Solid phase	
Mass flow	0.9686 [kg s^{-1}]
Velocity	22.475 [m s^{-1}]

Chapter 3

RESULTS AND DISCUSSION

3.1 Calculations results

The different values are calculated according to the parametric modeling seen in chapter 2, table 3.1 shows the different results.

Table 3.1: Parametric design BEP

Variable	Value
Q_d	58 [m^3/s]
H_d	213.4 [m]
P_d	121.4 [MW]
n	322.037 [rpm]
n_s	5038.83 [rpm]
ω	34.2716 [rad/s]
α_0	21.58°

The calculated data, the power, are compared with the experimental data in situ of the work carried out by Mora [43]. The discharge and height conditions were considered as input data. Table 3.2 shows the corresponding values for a flow rate of 58 [m3 / s] (BEP). An error of 12.32% is determined, The error is explained through the fact that the method is purely theoretical with a two-dimensional approach and does not consider irreversibilities . The result is acceptable for which we continue with the analysis of the case study.

Table 3.2: Validation procedure

Variables			
Q_{exp}[m^3/s]	$Power_{exp}$[MW]	$Power_{cal}[MW]$	%Error
58	103.18	115.9	12.32%

3.2 Drag analysis

In turbomachines,it is of interest that the drag is minimal. Therefore, an analysis of the NACA profiles is performed. The overall design is for the best efficiency point (BEP). However, it is important to verify the behavior of the GV profiles for different angles of attack around the BEP. This analysis allows selecting the profile that generates the least energy loss. Figure 3.1 shows the percentage variation of the Drag Coefficient (C_D) for various angles of attack. The NACA 0012, NACA 4412, NACA 5412 and NACA 6412 profiles are the subject of analysis.

The following observations are found.

- NACA 0012 has the lowest variation of C_D. In the range of -30 to 0 degrees, compared to the other profiles. Therefore, it is the most desirable to implement for the GV in the specified range.

- The asymmetric NACA profiles have the minimum variation of the C_D compared to the symmetrical NACA 0012 profile. The asymmetric profiles generate less turbulence for high Reynolds numbers. This behavior occurs in the range of -30 to -20 degrees.

- The NACA 0012 profile has an undesirable behavior in the range of 0 to 30 degrees. It shows a great variation of the C_D compared to the asymmetric profiles. Asymmetric profiles have slight C_D variations. Therefore, in a range of back rake angles a symmetric profile, NACA 0012, is desirable. However, for positive rake angles asymmetric profiles are desirable. Additional analysis is required to select a profile for the GV.

3.3 Erosion analysis

An analysis of the fluid velocity is performed along the camber line. The curvature of the asymmetrical NACA profiles changes the direction of speed at the GV outlet. The analysis is performed along this line,(see figure 3.3) in order to capture the fluid path between the

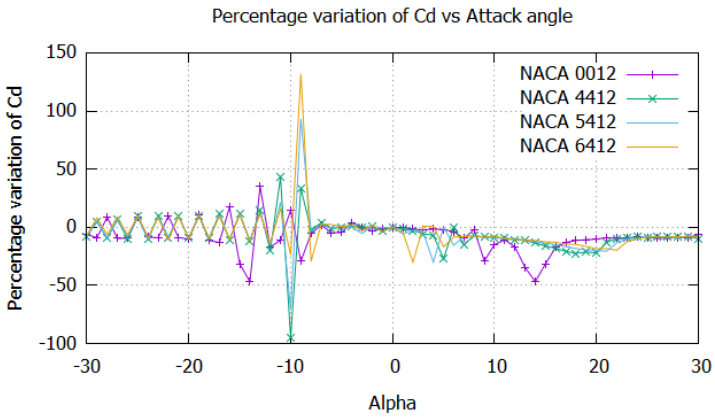

Figure 3.1: C_D variation for NACA profiles(Source: Own)

suction side and pressure side of the NACA profile. Figure 3.2 shows the existing deflection in the profiles. Clearly the NACA 0012 profile has no deflection as it is symmetrical. The NACA profiles 4412, 5412 and 6412 have a marked deflection.

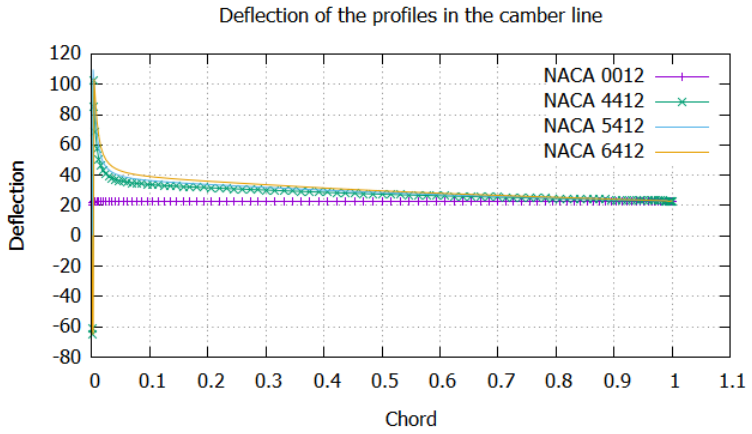

Figure 3.2: Deflection of the camber line (Source: Own)

The fluid velocity shows changes for the asymmetric profiles compared to the NACA 0012 profile. The changes appear both in their magnitude and in their direction, which is determined as a function of their curvature. The most notable change occurs in the NACA 6412 profile then in the NACA 5412 and 4412 profiles as shown in the figure 2.4.

The curvature of the asymmetric profiles deflects the fluid at the runner inlet. Therefore,

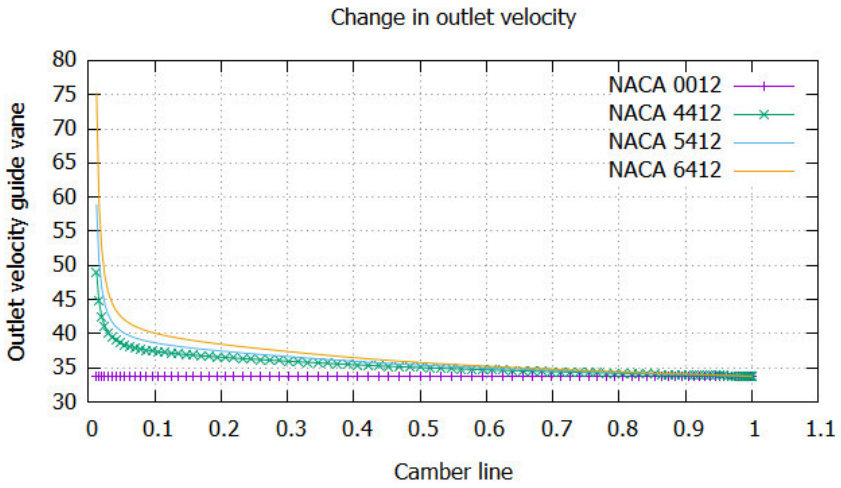

Figure 3.3: Outlet velocity magnitude guide vane (Source: Own)

the solid particles that hit the runner blades change their angle of impact. Figure 3.4 shows the estimate of the Erosion factor (E_f). NACA profile 0012 is the reference design. NACA 4412, 5412 and 6412 show a lower Erosion factor since their asymmetry changes the relative speed. NACA 6412 profile has the least E_f

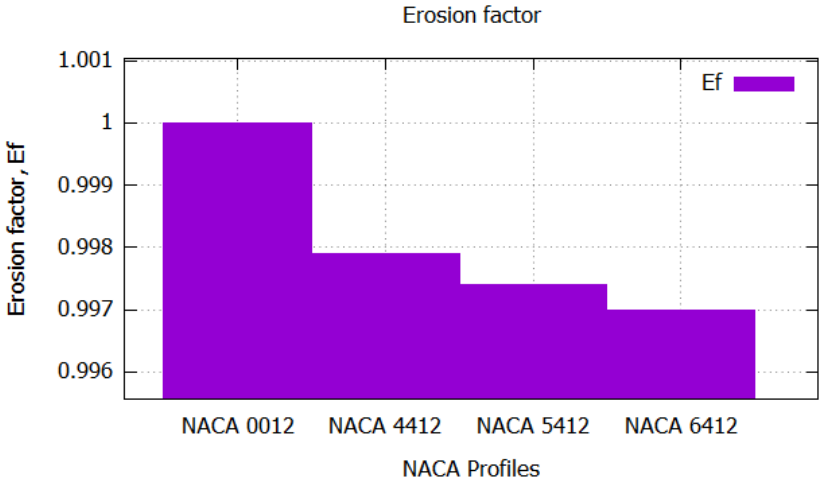

Figure 3.4: Erosion factor E_f (Source: Own)

3.4 Analysis of erosion in the guide vanes and runner of the Francis turbine

3.4.1 Flow analysis

Figure 3.5 shows the pathlines of the velocity magnitude for the different configurations. Figure 3.5a is referenced with the NACA profile 0012. Figures 3.5b, 3.5c and 3.5d with asymmetric profiles show changes in their velocity path compared to Figure 3.5a. Fluid path changes are observed at guide vanes outlet in asymmetric profiles compared to NACA 0012. Asymmetric profiles change fluid path slightly at runner inlet. The change in the fluid path leads to a reduction in erosion in guide vanes and runner blades. As can be seen in the table 3.3, the variation in power is minimal between the different configurations. It is concluded that the change of the profile does not affect the operation of the turbine and only causes erosion to be minimal.

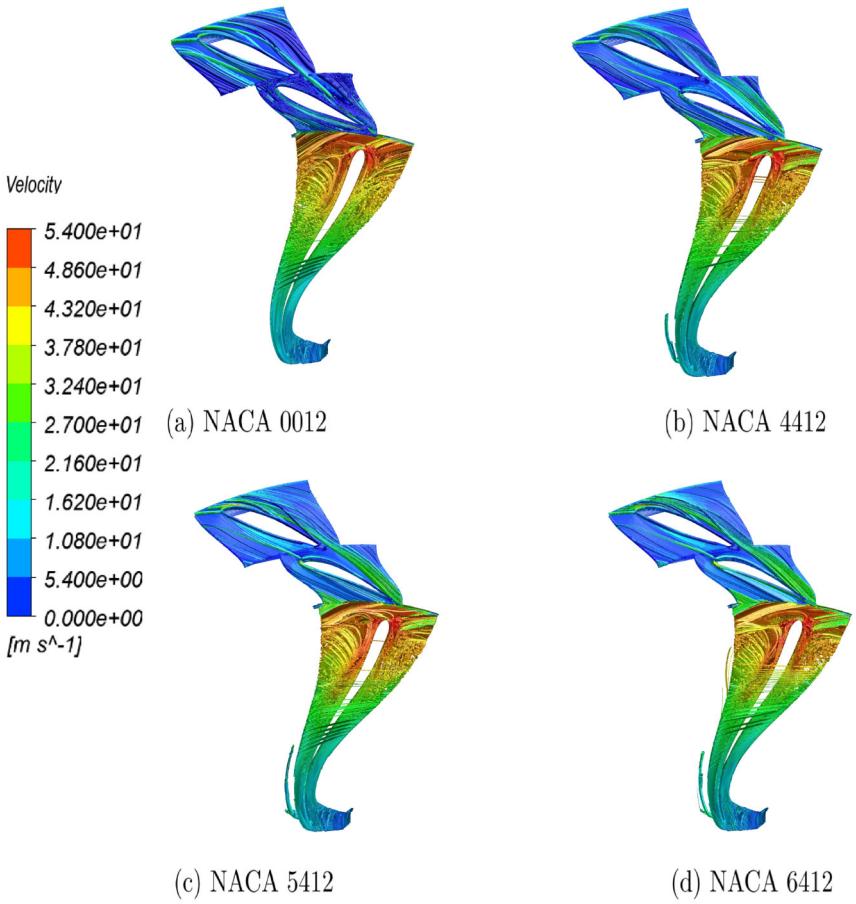

Figure 3.5: Velocity pathlines (Source: Own)

Profile	Power estimation[W]
NACA 0012	115962304.85
NACA 4412	115960563.50
NACA 5412	115962720.69
NACA 6412	115973116.78

Table 3.3: Power estimation

3.4.2 Guide vanes erosion analysis

Figure 3.6 shows the erosion in the guide vanes (GV) with the different profiles used.The NACA 0012 profile is the reference for erosion analysis in the other profiles. Near the hub and shroud you can see areas very marked by the detachment of material, areas of red color, as shown in figure 3.6a. In the center zone, of the GV there is no detachment of material. Gradual wear is displayed all the way to the extremities of the GV surface.

NACA profile 4412 shows less wear compared to the NACA profile 0012. Only a tiny

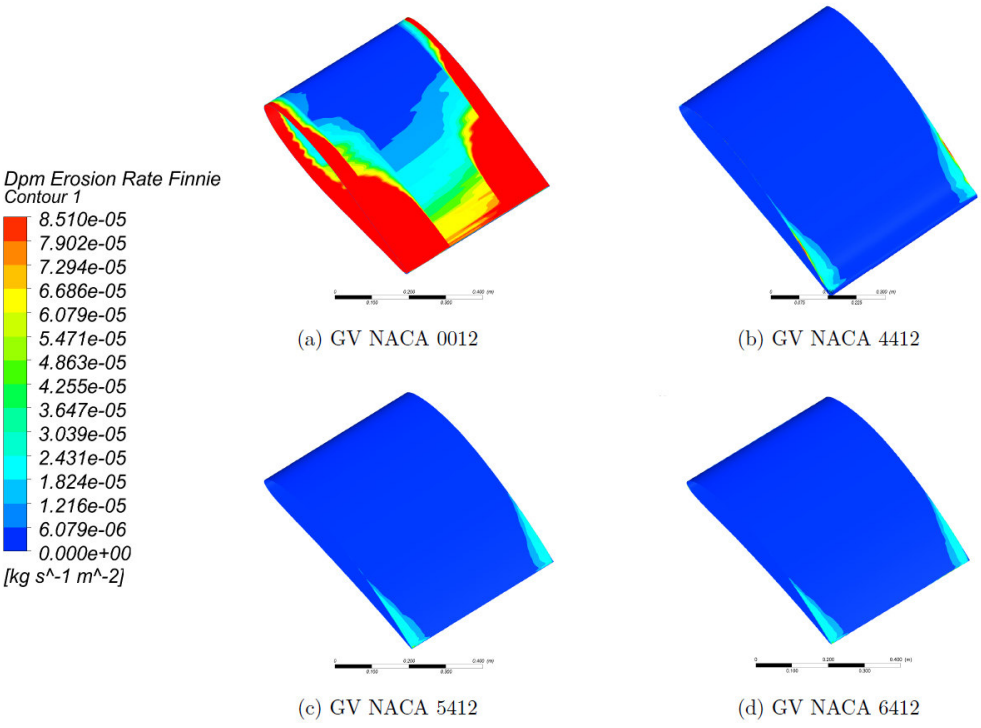

(a) GV NACA 0012 (b) GV NACA 4412

(c) GV NACA 5412 (d) GV NACA 6412

Figure 3.6: Sediment erosion GV (Source: Own)

red stripe shows aggressive material shedding, as shown in figure 3.6b. At the exit of the GV a slight detachment of material can be observed at the ends of the surface.

NACA profiles 5412 and 6412 show a minimal area affected by erosion at the guide vane outlet compared to the NACA 0012 profile, as shown in the figure 3.6c and 3.6d.

Asymmetric profiles show minimal areas affected by erosion compared to the symmetric reference profile. It is concluded that the asymmetric profiles are more suitable for use in

the study case.

3.4.3 Guide vanes effect on runner blade erosion

The runner is the most expensive component in Francis turbines. Therefore, changing this item or performing maintenance work are precautionary tasks.

GVs have a direct influence on erosion in runner blades. The GV directs the fluid to the entrance of the runner. Figure 3.7 shows the erosion of the runner blades (RB) on the pressure side (PS) and suction side (SS). Figure 3.7a and 3.7b show the erosion caused by the impact of the particles when using a NACA 0012 profile in the GVs. This figure is the reference to compare with the other profiles. It can be seen that there is a detachment of material in the suction side and pressure side at the ends of the surface.

For the NACA profile 4412 the pressure side in the runner vane shows less eroded area compared to RV NACA profile 0012, as shown in the figure 3.7c and 3.7d. The suction side shows mid-surface erosion.

For the configuration with the NACA profile 5412, RV shows a similar eroded area compared to the NACA profile 0012 on the pressure side, as shown in the figure 3.7e and 3.7f. In the suction side near the hub and shroud there are areas marked by erosion. On the middle surface there are signs of slight erosion.

Finally, the configuration with the NACA profile 6412. RB presents a smaller area affected by erosion in the pressure side compared to the use of the NACA profile 0012, as shown in figure 3.7g and 3.7h. The suction side presents marked erosion at the ends of the surface greater than for the configuration with the NACA profile 0012 as shown in figure.

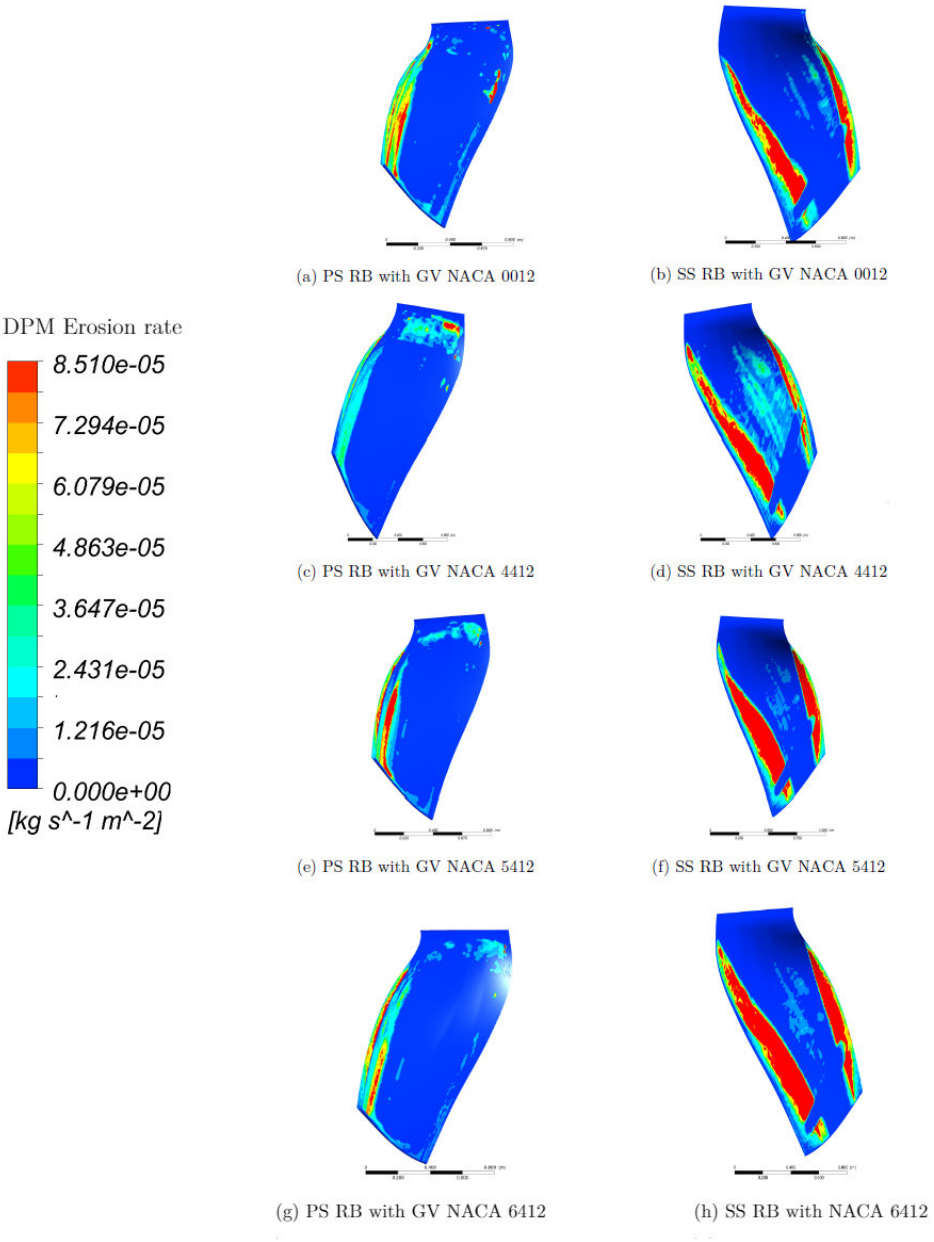

(a) PS RB with GV NACA 0012

(b) SS RB with GV NACA 0012

(c) PS RB with GV NACA 4412

(d) SS RB with GV NACA 4412

(e) PS RB with GV NACA 5412

(f) SS RB with GV NACA 5412

(g) PS RB with GV NACA 6412

(h) SS RB with NACA 6412

Figure 3.7: DPM Erosion rate (Source: Own)

3.4.4 Comparison with the case of study

The figure 3.8 shows the erosion in the San Francisco Hidropower plant guide vanes and the result obtained by the use of CFD. The NACA profile 0012 is the one currently used in the Francis turbine. As can be seen, there is quite a marked damage along the surface of the guide vane, especially at the ends. The result of the simulation shows that it is reliable and approximate to reality, therefore the results obtained in this work may be applicable to implement improvements in the turbine.

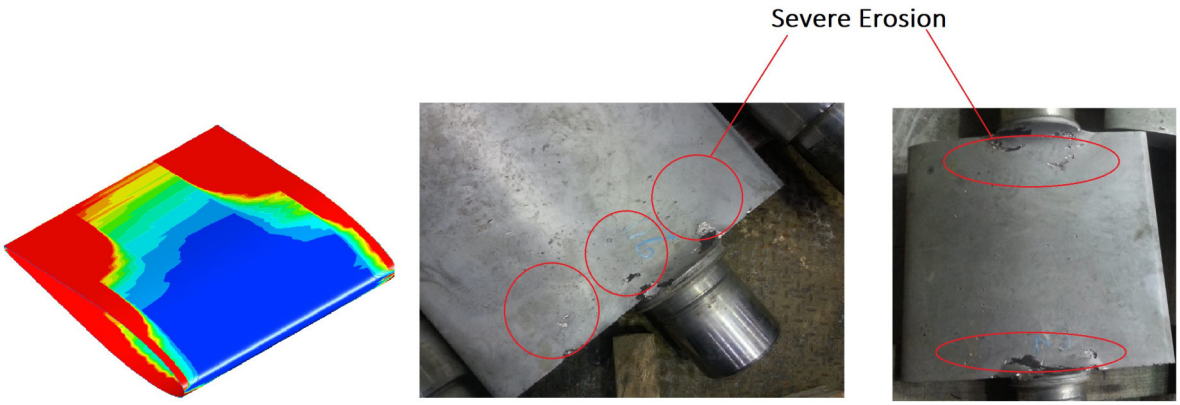

Figure 3.8: Guide vane erosion (Source: Own)

Chapter 4

CONCLUSIONS AND FUTURE WORK

4.1 Conclusions

Design of Francis turbine guide vanes to minimize the erosion produced by the impact of the liquid-solid biphasic flow has been carried out considering a parametric design, non-dimensional analysis, erosion assessment and numerical analysis.

A methodology was developed that allows designing the profile of the guide vanes under real operating conditions. The use of computational tools and the use of commercial CFD codes in Ansys Fluent allow to obtain reliable results in a short time. The TurboGrid software allows to obtain meshes in very short times according to the user's needs.

Four NACA profiles were selected for the analysis: NACA 0012, 4412, 5412 and 6412. The NACA 0012 profile is the one currently used in the case study, therefore it is the reference in each analysis.

Asymmetric profiles show better performance in GVs compared to the NACA 0012 profile. The variation of C_D in the four profiles under analysis is similar. The calculated Erosion Factor shows that asymmetric profiles tend to reduce erosion in runner blades. NACA profile 6412 has the lowest E_f.

The mesh of approximately 6.3 million nodes meets the stability and quality criteria for the $k-\omega$ SST numerical model. It shows reliable results as it meets the criteria for mesh independence, mass conservation and $y+$.

From the results obtained in the simulation in steady state, the following observations can be seen: the guide vane with the NACA profile 0012 presents quite marked erosion effects on its surface. Near the Hub and Shroud the erosion is very noticeable. The asymmetric profiles NACA 4412, 5412 and 6412 show reduced erosion only at the exit of the GV compared with the NACA 0012. This result is in accordance with previous works carried out by different authors on the same topic.

Guide vanes have a direct effect on the erosion on runner blades. The use of the NACA 4412 profile shows a reduction in pressure side and suction side erosion in the runner blade compared to the symmetrical profile. NACA 5412 shows similar erosion in the runner blade on the pressure side and marked erosion on the suction side compared to the NACA 0012

profile. Finally, NACA profile 6412 shows a smaller affected area on the runner blade on the pressure side, however, the suction side shows an area very marked by erosion compared to the use of NACA 0012.

4.2 Future work

The present work presents results which are reason for discussion. An analysis is presented with a different approach to the topic. Therefore it allows to propose new alternatives to design. It is intended to address new case studies following the methodology used. In addition, it is intended to carry out experimental research in order to strengthen the investigative work.

Bibliography

[1] "Energía Hidroeléctrica – CIE." http://energia.org.ec/cie/energia-hidroelectrica/ (accessed Jan. 22, 2021).

[2] P. Moncayo and M. D. Espinoza, "Parque Arqueológico Cochasquí," p. 168.

[3] AGENCIA DE REGULACION Y CONTROL DE ELECTRICIDAD."Estadistica Anual y Multianual de Sector Eléctrico Ecuatoriano" (2017)

[4] Chitrakar, S., Dahlhaug, O. G., Neopane, H. P. (2018). Numerical investigation of the effect of leakage flow through erosion-induced clearance gaps of guide vanes on the performance of Francis turbines. Engineering Applications of Computational Fluid Mechanics, 12(1), 662-678. https://doi.org/10.1080/19942060.2018.1509806

[5] Koirala, R., Neopane, H. P., Shrestha, O., Zhu, B., Thapa, B. (2017). Selection of guide vane profile for erosion handling in Francis turbines. Renewable Energy, 112, 328-336. https://doi.org/10.1016/j.renene.2017.05.033

[6] Lama, R., Dahal, D. R., Gautam, S., Acharya, N., Neopane, H., Thapa, B. S. (2018). Numerical investigation on performance and sediment erosion of Francis runner with different guide vane profiles. Journal of Physics: Conference Series, 1042, 012004. https://doi.org/10.1088/1742-6596/1042/1/012004

[7] Nora, L. P. (s. f.). Study of sediment erosion in guide vanes of Francis turbine. 85.

[8] R. Koirala, B. Thapa, H. P. Neopane, and B. Zhu, "A review on flow and sediment erosion in guide vanes of Francis turbines," Renewable and Sustainable Energy Reviews, vol. 75, pp. 1054–1065, Aug. 2017, doi: 10.1016/j.rser.2016.11.085.

[9] B. S. Thapa, O. G. Dahlhaug, and B. Thapa, "Sediment erosion in hydro turbines and its effect on the flow around guide vanes of Francis turbine," Renewable and Sustainable Energy Reviews, vol. 49, pp. 1100–1113, Sep. 2015, doi: 10.1016/j.rser.2015.04.178.

[10] N. Acharya, C. Trivedi, N. M. Wahl, S. Gautam, S. Chitrakar, and O. G. Dahlhaug, "Numerical study of sediment erosion in guide vanes of a high head Francis turbine," J. Phys.: Conf. Ser., vol. 1266, p. 012004, Jun. 2019, doi: 10.1088/1742-6596/1266/1/012004.

[11] "Synergism between Corrosion and Abrasive Wear — International Tribology Conference 1987, Melbourne, 2-4 December 1987: Preprints of Papers." https://search.informit.org/doi/abs/10.3316/informit.435097919063393 (accessed Jun. 08, 2021).

[12] G. A. Dahl, "Hydraulic design of a Francis turbine that will be influenced by sediment erosion," p. 149.

[13] Guide on How to Develop a Small Hydropower Plant, European Small Hydropower Association – ESHA, 2004.

[14] Okyay, G. (n.d.). A THESIS SUBMITTED TO THE GRADUATE SCHOOL OF NATURAL AND APPLIED SCIENCES OF MIDDLE EAST TECHNICAL UNIVERSITY. 124.

[15] Thapa, B. S., Thapa, B., Dahlhaug, O. G. (2012). Current research in hydraulic turbines for handling sediments. Energy, 47(1), 62–69. https://doi.org/10.1016/j.energy.2012.05.014

[16] Bone Fonte E.(2017).Metodología de Diseño para una Turbina Francis Mediante Diseño Paramétrico, Optimización Multiobjetivo y Simulación en CFD (Master's thesis, Escuela Politécnica Nacional)

[17] "16.10.5. Accretion."https://ansyshelp.ansys.com/account/secured?returnurl=/Views/Secured/corp/v195 /$flu_th/flu_ths_{ect_d}pm_eros_a$ccre.html (accessed Aug. 19, 2021).

[18] "16.10.3.McLaury Erosion Model." https://ansyshelp.ansys.com/Views/Secured/corp/v195/fl$u_th/flu_ths_{ec_d}iscrete_erosion_m$claury.html (accessed Aug. 19, 2021).

[19] "16.10.1. Finnie Erosion Model." https://ansyshelp.ansys.com/Views/Secured/corp/v195/fl$u_th/flu_ths_{ec_d}iscrete_erosion_f$innie.html (accessed Aug. 19, 2021).

[20] "16.10.2. Oka Erosion Model." https://ansyshelp.ansys.com/Views/Secured/corp/v195/fl$u_th/flu_ths_{ec_d}iscrete_erosion_o$ka.html
(accessed Aug. 19, 2021).

[21] Drew D A. Mathematical Modeling of Two-Phase Flow. Annual Review of Fluid Mechanics, 1983, 15.

[22] Frawley P, O'Mahony P, Geron M. Comparison of Lagrangian and Eulerian Simulations of Slurry Flows in a Sudden Expansion. Journal of Fluids Engineering, 2010, 132(9): 91301.

[23] Apte S V, Mahesh K, Lundgren T. A Eulerian-Lagrangian model to simulate two-phase / particulate flows. Center for Turbulence Research: Annual Research Briefs, 2003: 161–171.

[24] Grigoriadis D G, Kassinos S C. Lagrangian particle dispersion in turbulent flow over a wall mounted obstacle. International Journal of Heat and Fluid Flow, 2009, 30(3): 462–470.

[25] Neopane H. Sediment erosion in hydro turbines[D]. Norwegian University of Science and Technology, 2010.

[26] Thapa B S, Dahlhaug O G, Thapa B. Sediment erosion in hydro turbines and its effect on the flow around guide vanes of Francis turbine. Renewable and Sustainable Energy Reviews, 2015, 49: 1100–1113.

[27] Eltvik Mette. Sediment erosion in Francis turbines[D]. Norwegian University of Science and Technology, 2013.

[28] Sommerfeld M, Ando A, Wennerberg D. Swirling, particle-laden flows through a pipe expansion. ASME Journal Fluids Engineering, 1992, 114(4): 648–656.

[29] Crowe, C., Sommerfeld, M., Tsuji Y. Multiphase Flows with Droplets and Particles. CRC Press, Boca Raton, .

[30] Lai A C K, Chen F Z. Comparison of a new Eulerian model with a modified Lagrangian approach for particle distribution and deposition indoors. Atmospheric Environment, 2007, 41(25): 5249–5256.

[31] Li A, Ahmadi G. Dispersion and deposition of spherical particles from point sources in a turbulent channel flow. Aerosol Sci. Technol., 1992, 16: 209–226.

[32] Crowe C T, Trougtt T R, Chung J N. numerical model for two phase turbulence flow. Annual Review of Fluid Mechanics, 1996, 28(1): 11–43.

[33] Guha A. Transport and Deposition of Particles in Turbulent and Laminar Flow. Annual Review of Fluid Mechanics, 2008, 40(1): 311–341.

[34] Drew D A. Effect of particle velocity fluctuations in fluid particle flows. Physica A, 1991, 179: 69–8.

[35] Shuen J ., Solomon A S P, Zhang Q ., et al. Structure of particle-laden jets: measurements and predictions. AIAA Journal, 1985, 13: 396–404.

[36] Elghobashi S E, Truesdell G C. On the two- way interaction between homogeneous turbulence and dispersed solid particles I: turbulence modification. Physics of Fluids A :Fluid Dynamics, 1993, 5(7): 1790–1801.

[37] Saber A, Lundström T S, Hellström J G I. Turbulent Modulation in Particulate Flow : A Review of Critical Variables. Engineering, 2015, 7: 597–609.

[38] Lain S, Sommerfeld M. Turbulence modulation in dispersed two-phase flow laden with solids from a Lagrangian perspective. International Journal of Heat and Fluid Flow, 2003, 24(4): 616–625.

[39] Gore R A, Crowe S T. Effect of particle size on modulating turbulence intensity. Int. J. Multiphase Flow, 1989, 15: 279–285.

[40] Volavy J, Forman M, Jicha M. Turbulence modulation by particles in Large Eddy Simulation of backward-facing step flow. Journal of Physics: Conference Series, 2011, 318: 52023.

[41] "Ansys Fluent — Fluid Simulation Software." https://www.ansys.com/products/fluids/ansys-fluent (accessed Aug. 20, 2021).

[42] "SAN FRANCISCO." https://www.celec.gob.ec/hidroagoyan/index.php/centrales/san-francisco (accessed Oct. 10, 2020).

[43] Mora, M. C. A. (n.d.). TRABAJO DE TITULACIÓN PREVIO A LA OBTENCIÓN DEL TÍTULO DE MAGÍSTER EN DISEÑO, PRODUCCIÓN Y AUTOMATIZACIÓN INDUSTRIAL. 81.

[44] SN Power. Presentation of the energy situation in South America. SN Power office, Santiago, Chile. 2009.

[45] Golden Associates Inc., Estudios para mejorías en el embalse de la presa de Agoyan-mitigacion de sedimentos sólidos y flotantes, Hidropastaza Proyecto San Francisco Baños de Agua Santa Ecuador, Colorado 80228 USA: 44 Union Bloulevard, Suite 300. Diciembre 20 del 2010

[46] E. Cando, "Sediment erosion prediction in Francis turbines based on liquid-solid two-phase flow", Tsinghua University, China, 2018.

[47] Yanez J. "Diseño paramétrico de álabes para turbinas Francis". Escuela Politécnica Nacional, Facultad de Ingeniería Mecánica, 2017.

[48] Gjøsæter K. “Hydraulic Design of Francis Turbine Exposed to Sediment Erosion”. Norwegian University of Science and Technology, 2011.

[49] “CENTRALES HIDROELÉCTRICAS DEL ECUADOR.” https://observatorioelc.ister.edu.ec/2021/04/26/centrales-hidroelectricas-del-ecuador/ (accessed Sep. 17, 2021).

[50] Drew D A. Mathematical Modeling of Two-Phase Flow. Annual Review of Fluid Mechanics, 1983, 15.

[51] Apte S V, Mahesh K, Lundgren T. A Eulerian-Lagrangian model to simulate two-phase / particulate flows. Center for Turbulence Research: Annual Research Briefs, 2003: 161–171.

[52] Bardal Einar. Corrosion and protection. Springer Science Business Media; 2004.

[53] Padhy MK, Saini RP. Effect of size and concentration of silt particles on erosion of Pelton turbine buckets”. Energy 2009;34(10):1477e83.

[54] Padhy MK, Saini RP. Study of silt erosion on performance of a Pelton turbine”. Energy 2011;36(1):141e7.

[55] Tsuguo N. Estimation of repair cycle of turbine due to abrasion caused by suspended sand and determination of desilting basin capacity”. In: Proceedings of the international seminar on sediment handling technique, NHA, Kathmandu; 1999.

[56] IEC. Hydraulic turbines, storage pumps and pump turbines-model acceptance tests. British Standard Institution; 1999. Tech. rep.

[57] J. H. Masoodi and G. A. Harmain, “A methodology for assessment of erosive wear on a Francis turbine runner,” Energy, vol. 118, pp. 644–657, Jan. 2017, doi: 10.1016/j.energy.2016.10.095.

Appendices

.1 Appendix 1

Lines of code in Python

```
from math import cos, sin, tan
from math import atan
from math import pi
from math import pow
from math import sqrt

    def linspace(start,stop,np):

    return [start+(stop-start)*i/(np-1) for i in range(np)]

    def interpolate(xa,ya,queryPoints):

    number of points
n = len(xa)
u, y2 = [0]*n, [0]*n

    for i in range(1,n-1):

    This is the decomposition loop of the tridiagonal algorithm.
y2 and u are used for temporary storage of the decomposed factors.

    wx = xa[i + 1] - xa[i - 1]
sig = (xa[i] - xa[i - 1]) / wx
p = sig * y2[i - 1] + 2.0

    y2[i] = (sig - 1.0) / p

    ddydx = (ya[i + 1] - ya[i]) / (xa[i + 1] - xa[i]) - (ya[i] - ya[i - 1]) / (xa[i] - xa[i - 1])

    u[i] = (6.0 * ddydx / wx - sig * u[i - 1]) / p

    y2[n - 1] = 0

    for i in range(n-2,-1,-1): y2[i] = y2[i] * y2[i + 1] + u[i]
results = [0]*n

    for i in range(len(queryPoints)):
```

```
    klo = 0
khi = n - 1

    while (khi - klo ¿ 1):
k = (khi + klo) » 1
if (xa[k] ¿ queryPoints[i]):
khi = k
else:
klo = k

    h = xa[khi] - xa[klo]
a = (xa[khi] - queryPoints[i]) / h
b = (queryPoints[i] - xa[klo]) / h

    results[i] = a * ya[klo] + b * ya[khi] + ((a * a * a - a) * y2[klo] + (b * b * b - b) *
y2[khi]) * (h * h) / 6.0

    return results

    def naca4(number, n, finite$_TE$ = $False$, $half_cosine_s$pacing = False):
"""
$Returns 2 * n + 1 points in [0 1] for the given 4 digit NACA number string$
"""

    m = float(number[0])/100.0
p = float(number[1])/10.0
t = float(number[2:])/100.0

    a0 = +0.2969
a1 = -0.1260
a2 = -0.3516
a3 = +0.2843

    if finite$_TE$ :
$a4 = -0.1015$ $For finite thick TE$
$else$ :
$a4 = -0.1036 For zero thick TE$

    if $half_cosine_spacing$:
beta = linspace(0.0,pi,n+1)
```

x = $[(0.5 * (1.0 - cos(xx)))forxxinbeta]Halfcosinebasedspacing$
else:
x = linspace(0.0,1.0,n+1)

    yt = [5*t*(a0*sqrt(xx)+a1*xx+a2*pow(xx,2)+a3*pow(xx,3)+a4*pow(xx,4)) for xx in x]

    xc1 = [xx for xx in x if xx ¡= p]
xc2 = [xx for xx in x if xx ¿ p]

    if p == 0:
xu = x
yu = yt

    xl = x
yl = [-xx for xx in yt]

    xc = xc1 + xc2
zc = [0]*len(xc)
else:
yc1 = [m/pow(p,2)*xx*(2*p-xx) for xx in xc1]
yc2 = [m/pow(1-p,2)*(1-2*p+xx)*(1-xx) for xx in xc2]
zc = yc1 + yc2

    dyc1$_d$x = $[m/pow(p, 2) * (2 * p - 2 * xx)forxxinxc1]$
$dyc2_dx = [m/pow(1 - p, 2) * (2 * p - 2 * xx)forxxinxc2]$
$dyc_dx = dyc1_dx + dyc2_dx$

    theta = [atan(xx) for xx in dyc$_d$x]

    xu = [xx - yy * sin(zz) for xx,yy,zz in zip(x,yt,theta)]
yu = [xx + yy * cos(zz) for xx,yy,zz in zip(zc,yt,theta)]

    xl = [xx + yy * sin(zz) for xx,yy,zz in zip(x,yt,theta)]
yl = [xx - yy * cos(zz) for xx,yy,zz in zip(zc,yt,theta)]

    X = xu[::-1] + xl[1:]
Z = yu[::-1] + yl[1:]

    return X,Z

def naca5(number, n, finite$_TE = False, half_cosine_spacing = False$) :
"""
$Returns 2 * n + 1 points in [0 1] for the given 5 digit NACA 5 number string$
"""

naca1 = int(number[0])
naca23 = int(number[1:3])
naca45 = int(number[3:])

cld = naca1*(3.0/2.0)/10.0
p = 0.5*naca23/100.0
t = naca45/100.0

a0 = +0.2969
a1 = -0.1260
a2 = -0.3516
a3 = +0.2843

if finite$_TE$:
$a4 = -0.1015 For finite thickness trailing edge$
$else$:
$a4 = -0.1036 For zero thickness trailing edge$

if half$_cosine_spacing$:
$beta = linspace(0.0, pi, n + 1)$
$x = [(0.5 * (1.0 - cos(x))) for x in beta] Half cosine based spacing$
$else$:
$x = linspace(0.0, 1.0, n + 1)$

yt = [5*t*(a0*sqrt(xx)+a1*xx+a2*pow(xx,2)+a3*pow(xx,3)+a4*pow(xx,4)) for xx in x]

P = [0.05,0.1,0.15,0.2,0.25]
M = [0.0580,0.1260,0.2025,0.2900,0.3910]
K = [361.4,51.64,15.957,6.643,3.230]

m = interpolate(P,M,[p])[0]
k1 = interpolate(M,K,[m])[0]

xc1 = [xx for xx in x if xx ¡= p]
xc2 = [xx for xx in x if xx ¿ p]
xc = xc1 + xc2

if p == 0:
xu = x
yu = yt

xl = x
yl = [-x for x in yt]

zc = [0]*len(xc)
else:
yc1 = [k1/6.0*(pow(xx,3)-3*m*pow(xx,2)+ pow(m,2)*(3-m)*xx) for xx in xc1]
yc2 = [k1/6.0*pow(m,3)*(1-xx) for xx in xc2]
zc = [cld/0.3 * xx for xx in yc1 + yc2]

$dyc1_dx = [cld/0.3 * (1.0/6.0) * k1 * (3 * pow(xx, 2) - 6 * m * xx + pow(m, 2) * (3 - m))forxxinxc1]$
$dyc2_dx = [cld/0.3 * (1.0/6.0) * k1 * pow(m, 3)] * len(xc2)$

$dyc_dx = dyc1_dx + dyc2_dx$
$theta = [atan(xx)forxxindyc_dx]$

xu = [xx - yy * sin(zz) for xx,yy,zz in zip(x,yt,theta)]
yu = [xx + yy * cos(zz) for xx,yy,zz in zip(zc,yt,theta)]

xl = [xx + yy * sin(zz) for xx,yy,zz in zip(x,yt,theta)]
yl = [xx - yy * cos(zz) for xx,yy,zz in zip(zc,yt,theta)]

X = xu[::-1] + xl[1:]
Z = yu[::-1] + yl[1:]

return X,Z

def naca(number, n, $finite_TE = False, half_cosine_spacing = False$) :
if $len(number) == 4$:
return $naca4(number, n, finite_TE, half_cosine_spacing)$
elif len(number)==5:
return naca5(number, n, $finite_TE, half_cosine_spacing$)

else:
raise Exception

class Display(object):
$def_{init_{(self):}}$
import matplotlib.pyplot as plt
self.plt = plt
self.h = []
self.label = []
self.fig, self.ax = self.plt.subplots()
self.plt.axis('equal')
self.plt.xlabel('x')
self.plt.ylabel('y')
self.ax.grid(True)
def plot(self, X, Y,label=''):
h, = self.plt.plot(X, Y, '-', linewidth = 1)
self.h.append(h)
self.label.append(label)
def show(self):
self.plt.axis((-0.1,1.1)+self.plt.axis()[2:])
self.ax.legend(self.h, self.label)
self.plt.show()

def demo(profNaca = ['4412'], nPoints = 240, finite$_T E = False, half_cosine_spacing = False$) :

d = Display()
for i,p in enumerate(profNaca):
X,Y = naca(p, nPoints, finite$_T E, half_cosine_spacing$)
$d.plot(X, Y, p)$
$d.show()$

def main():
import os
from argparse import ArgumentParser, RawDescriptionHelpFormatter
from textwrap import dedent
parser = ArgumentParser(
$formatter_class = RawDescriptionHelpFormatter$,
description = dedent('''
Script to create NACA4 and NACA5 profiles

If no argument is provided, a demo is displayed.
”’),
epilog = dedent(”’

$'''.format(os.path.basename(_{file}))))$
$parser.add_argument('-p','--profile', type = str,$
help = 'Profile name or set of profiles names separated by spaces. Example: ”0009”, ”0009 2414 6409”’)
parser.add$_{a}rgument$('-n','–nbPoints', type = int, default = 120,
$help =' Numberofpointsusedtodiscretizechord.Profilewillhave2*nbPoints+1dots.Defaultis120.')$
$parser.add_argument('-s','–half_cosine_spacing', action =' store_true',$
help = 'Half cosine based spacing, instead of a linear spacing of chord. ’
'This option is recommended to have a smooth leading edge.')
parser.add$_{a}rgument$('-f','–finite$_{T}E', action =' store_true',$
help = 'Finite thickness trailing edge. Default is False, corresponding to zero thickness trailing edge.')
parser.add$_{a}rgument$('-d','–display', action = 'store$_{t}rue',$
help = 'Flag used to display the profile(s).')
$args = parser.parse_args()$
if args.profile is None:
demo($nPoints = args.nbPoints, finite_TE = args.finite_TE, half_cosine_spacing = args.half_cosine_sp$
else:
if args.display:
d = Display()
for p in args.profile.split(' '):
X,Y = naca($p, args.nbPoints, args.finite_TE, args.half_cosine_spacing$)
d.plot(X, Y, p)
d.show()
else:
for p in args.profile.split(' '):
X,Y = naca($p, args.nbPoints, args.finite_TE, args.half_cosine_spacing$)
for x,y in zip(X,Y):
print(x,y)

$if_{name}==''_{main}':$
main